3 Proposed Facility

This Section describes the NSLS-II user facility that BNL proposes to design, construct, and operate. Section 3.1.1 summarizes the light source capabilities required to enable the science described in Section 2. Section 3.1.2 summarizes the characteristics and capabilities of the current NSLS X-ray and VUV/IR storage rings to illustrate both the need for a new X-ray source (as opposed to an upgrade of the existing one) and also the tremendous advance that NSLS-II represents. Section 3.2 describes several alternative approaches for meeting the requirements, including free electron lasers, energy recovery linacs, and third generation storage rings. From these considerations, it is clear that an advanced third generation X-ray storage ring, designed to be upgradeable to future operation as an energy recovery linac, is the best choice for NSLS-II. A pre-conceptual design for NSLS-II and its expected performance are described in Section 3.3. The design of NSLS-II will be highly aggressive in order to deliver the necessary superlative characteristics, and will set a new standard for third generation light sources. The various design considerations and challenges necessary to realize this goal are reviewed in Section 3.4. The potential to be upgraded in the future to operate as an energy recovery linac, for even greater performance, is a key distinguishing characteristic of NSLS-II. The design considerations to enable that option are described in Section 3.5. Section 3.6 closes this Section with a discussion of the facility siting considerations and of compatibility with BNL's Site Master Plan.

3.1 Capability Requirements

3.1.1 Requirements for NSLS-II

In Section 2, we have outlined the range of current and future problems of interest in the many areas of science served by synchrotron radiation, including the most difficult, so-called grand challenge problems. To address those scientific challenges, it is necessary to

- probe materials on ever smaller length scales, down to 10 nanometers or less
- apply a number of new techniques based on utilizing the coherence of the photons
- study elementary excitations with energies ranging from < 1 meV to ~ 10 eV
- access resonance and absorption edges ranging from ~ 100 eV to ~ 10,000 eV

The photon qualities needed to enable these capabilities determine the design goals for the NSLS-II light source. These goals are:

- highest possible time average brightness, 10,000 times more than the current NSLS and more than any other current or planned source in the energy range 0.3 to 20 keV
- highest possible flux, 10x more than the current NSLS, and more than any other current or planned source in the energy range 0.3 to 20 keV
- photon pulse lengths down to 11 psec, 13 times shorter than the current NSLS
- wide spectral coverage, including the far-IR, UV, VUV, soft X-ray, and hard X-ray regions
- exquisite intensity, position, and pointing stability

A light source meeting these design goals will not only exceed the performance of the existing NSLS storage rings by many orders of magnitude but will also be a world leader in many characteristics, including highest average brightness and flux in the 0.3 to 20 keV energy range and exquisite stability.

3.1.2 Capabilities of Present NSLS

A photo of the exterior of the present NSLS building is shown in Figure 3.1.1. It houses two electron storage rings and their associated injection system consisting of a linear accelerator and a booster synchrotron. An interior diagram showing their layout and also that of the beamlines and associated laboratories is shown in Figure 3.1.2. The parameters of the X-ray ring and VUV/IR ring are given in Table 3.1.1.

The NSLS facility consists of two so-called second generation storage rings, having begun operation in 1982 as the first facility in the U.S. that was designed expressly for the use of synchrotron radiation. It was designed in the 1970's with the pioneering Chasman-Green lattice, which was developed at BNL, and utilizes double achromatic bends to provide zero-dispersion straight sections for insertion devices. It is optimized for brightness, within the constraints imposed by its small number of cells and small circumference, and includes only a small number of straight sections for insertion devices, which were still quite novel at that time. The two storage rings provide a wide range of photon energies, spanning from the far-IR to the hard X-ray (100 keV) range, that is still unique today.

The injection system consists of a 120 MeV electron linac that injects into a small (28 m circumference) booster synchrotron that accelerates the electrons up to 750 MeV. The booster serves as the injector for the VUV storage ring, which operates at 800 MeV to provide radiation in the infrared to soft X-ray region of the spectrum. The booster is also used to inject electrons into the X-ray storage ring, which operates at 2.8 GeV to provide hard X-rays.

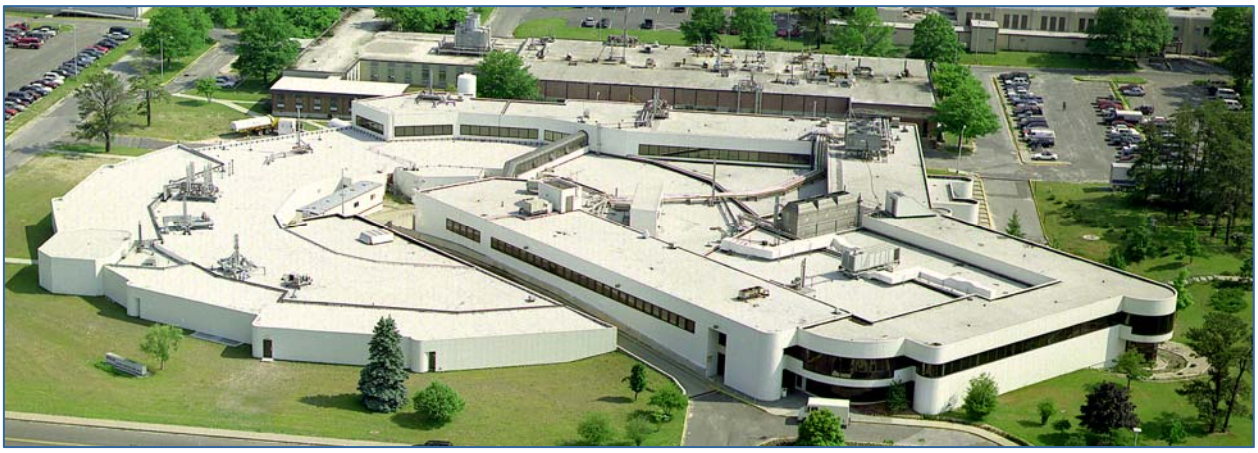

Figure 3.1.1 *Exterior view of the current NSLS facility. The VUV/IR ring is housed in the smaller square section extending out and to the lower right from the circular portion of the building, which houses the X-ray Ring.*

The 8 bending magnets and 4 straight sections on the VUV/IR ring host 30 beamlines. All beamlines are numbered clockwise starting from the U1 straight section. Only U5 and U13 host undulator insertion devices, with U1 used for injection and U9 occupied by two RF cavities.

The 16 bending magnets and 8 straight sections on the X-ray ring host 60 beamlines. These are also numbered clockwise starting from the X1 straight section. The beam is injected into the X5 straight, which hosts a nuclear physics gamma ray experiment (LEGS). Five other straights are fitted with insertion devices, feeding beamlines X1, X13, X17, X21, and X25. A total of four RF cavities are used, with two located in each of the X9 and X29 straights.

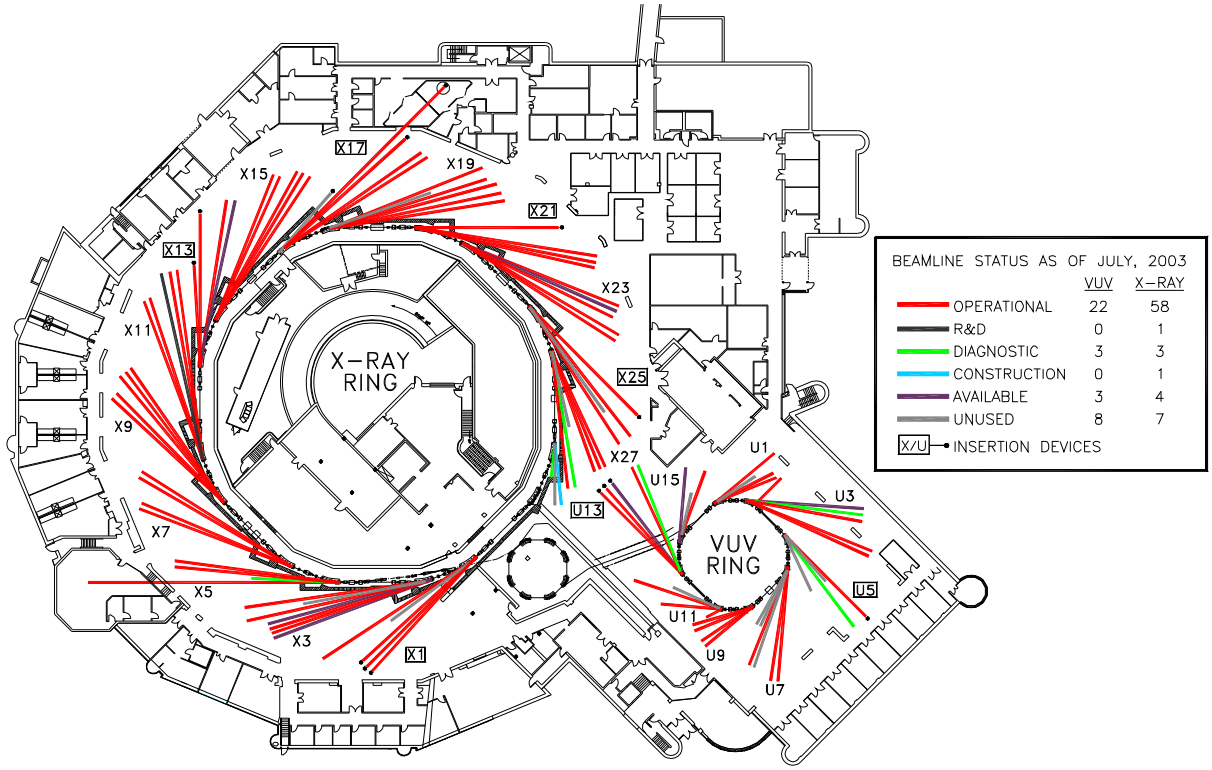

Figure 3.1.2 *Layout of X-ray ring, VUV/IR ring, booster, and experimental floor showing beamlines and associated setup laboratories.*

Parameter	X-ray Ring	VUV/IR Ring
Lattice Type	DBA	DBA
Circumference [m]	170	51
Superperiods	8	4
Number of Insertion Devices	5	2
Straight Section Length [m]	5	3
Energy [GeV]	2.8	0.8
Horizontal Emittance, ε_x [nm]	75	160
Emittance coupling, χ	0.002	0.025
Momentum Compaction, α	0.004	0.0235
Dipole Radius [m]	6.875	1.91
Bending Magnet Critical Energy [eV]	7091	600
ID Beta Functions, β_x, β_y [m]	1.60, 0.35	11.1, 5.84
RF Frequency [MHz]	52.88	52.88
Current at fill [mA]	280	1000
Average Current [mA]	238	665
Lifetime [Hours]	20	6
Revolution Frequency [MHz]	1.76	5.88
Orbit Time [nsec]	567	170
Maximum Number of RF Buckets	30	9
Typical Bunch Mode	25	7
Typical Single Bunch Current [mA]	11.2	143
Typical Single Bunch Charge [nC]	6.37	24.3
Bunch Length, σ [mm, ps]	43.5, 145	48.5, 162
Natural Energy Spread [%]	0.092	0.05

Table 3.1.1 *Parameters for the current NSLS X-ray and VUV/IR storage rings.*

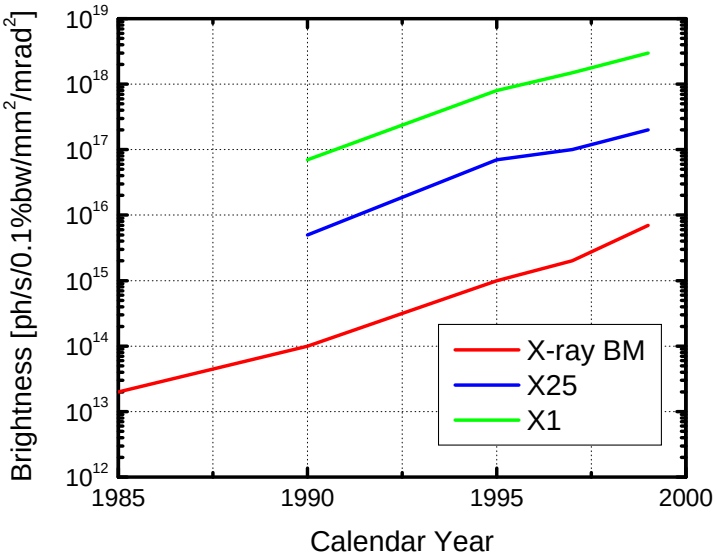

Figure 3.1.3 *Improvement in X-ray brightness over time from bending magnets, wiggler X25, and soft X-ray undulator X1.*

A concerted program of accelerator improvements over the last 20 years has steadily upgraded the

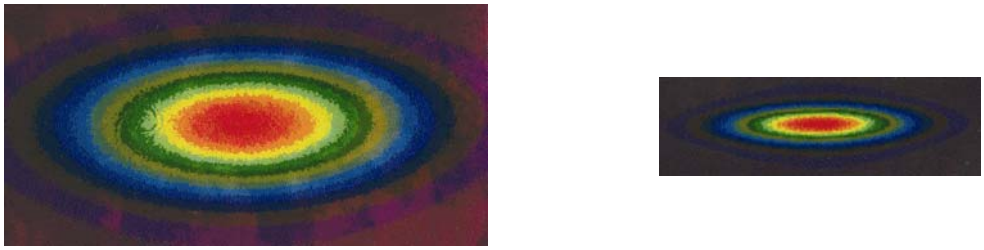

Figure 3.1.4 *Electron beam profile in the X-ray ring taken in 1990 (left) and in 2000 (right).*

performance of the NSLS to far surpass its original performance. Figure 3.1.3 shows the dramatic increase of five orders of magnitude in brightness of the brightest X-ray source at the NSLS over that period. About half of this gain was obtained by optimizing the storage ring lattice, resulting in a substantial reduction in electron emittance. For example, Figure 3.1.4 shows the reduction in electron beam size from 1990 to 2000. The other half of the gain in brightness was obtained by introducing advanced insertion devices, many of which were pioneered at the NSLS. These include development of a time varying (1 to 100 Hz) elliptically polarized wiggler and of in-vacuum undulators that operate with a full magnet gap down to 3.3 mm. Most recently, in replacing the RF cavities in the X9 and X29 straight sections with more reliable ones, they were also redesigned to allow room between them for installation of a short (0.3 m) Mini-gap in-vacuum undulator (MGU), as shown in Figure 3.1.5. The X29 MGU has been installed and the X29 beamline should become operational in the summer of 2004. Funding has just recently been provided to install an MGU in the X9 straight and build the X9 beamline.

Table 3.1.2 lists the full complement of insertion devices that the NSLS facility currently hosts or plans to host in the near future. These devices exhaust the useable straight sections and the NSLS is thus unable to add any additional high brightness beamlines beyond this set.

The NSLS and its successes served as a springboard for 'third-generation' storage ring facilities around the world. These designs are distinguished by having many more cells to obtain very low emittances and with many more straight sections to host insertion devices.

While the upgrade in performance that has been achieved with the NSLS is impressive, further improvements are not feasible. As outlined in Section 3.4.2, fundamental realities of accelerator physics require that the number of cells of the storage ring lattice be substantially increased in order to realize significant gains. We have considered ripping out the current X-ray storage ring and replacing it with a new lattice with 12 cells. However, this would provide only limited improvement and would require at least a two year shutdown, with a consequential serious negative impact on our large user community.

A new X-ray storage ring with a substantially larger circumference to accommodate many more cells and straight sections is necessary to meet the needs of the science case outlined in Section 2 for much higher brightness and flux in the VUV, soft X-ray, and hard X-ray energy ranges. Furthermore, by taking advantage of continued advances in storage ring technology, it is possible to surpass the performance of

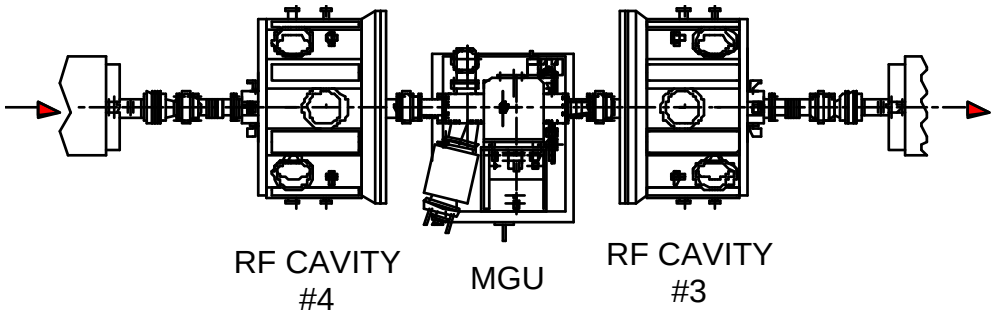

Figure 3.1.5 *Layout of X29 straight section, showing two RF cavities which were redesigned to allow insertion of a 0.3 m Mini-gap Undulator (MGU).*

Straight Section	Usage	Scientific Program
X1	Soft X-ray Undulator	Soft X-ray spectro-microscopy
X5	Injection	LEGS Nuclear Physics Gamma Ray Source
X9	RF plus Planned MGU	SAXS
X13	MGU plus Time Varing EPW	Magnetism plus X-ray Microprobe
X17	Superconducting Wiggler	High Pressure, Geoscience, Materials Science
X21	Hybrid Wiggler	Materials Science
X25	Hybrid Wiggler	Protein Crystallography
X29	RF plus MGU	Protein Crystallography
U1	Injection	Not usable
U5	UV Undualtor	Spin-resolved Photoemission, XES
U9	RF	Not usable
U13	UV Undulator	Photoemission

Table 3.1.2 *Straight sections on present NSLS X-ray and VUV/IR storage rings, their usage, including existing and planned insertion devices, injection and RF cavities, and the scientific programs they support. With the planned installation of the X9 MGU, straight sections usage will be at full capacity.*

existing or planned storage rings through the development and construction of a new state-of-the-art medium energy storage ring, serving many users simultaneously with world leading capabilities.

Due to incompatible accelerator physics requirements, it is not possible for the new X-ray storage ring to also provide very high brightness in the near- to far-IR region. Thus, in order to continue to provide world leading high brightness in this important spectral region, we propose relocating the existing VUV/IR storage ring to the area of the new X-ray storage ring and operating it solely as an IR source.

We propose to continue to operate the current NSLS X-ray ring for some period of overlap with the beginning of operations of the new X-ray ring. This will allow users time to move their programs over to the new facility. After all users have moved over, the old X-ray storage ring would be decommissioned and the building made available for other purposes.

3.2 Design Alternatives

There are three alternative approaches to generating radiation in the 0.3 to 20 keV energy range that either exist (third generation storage rings), are under development (free electron lasers) or have been proposed (energy recovery linacs). In this section, we consider these alternatives to meeting the needs of the science outlined in Section 2 and argue that a facility based on an advanced third generation storage ring, designed to be upgradeable to future operation as an energy recovery linac, is the best choice.

3.2.1 Free Electron Lasers

There are several free electron laser (FEL) projects that are either under construction or in advanced planning stages. In the U.S., DOE is funding the construction of the Linac Coherent Light Source (LCLS), which is being built at the Stanford Linear Accelerator Center (SLAC). In Europe, the XFEL and BESSY FEL projects are in advanced stages of planning. Representative of FELs, when operational in 2008 the LCLS will provide unprecedented peak (10^{32} ph/sec/0.1%bw/mm^2/mrad^2) and time average (10^{22} ph/sec/0.1%bw/mm^2/mrad^2) brightness and ultrashort (230 fsec or less) pulses at a maximum rate of 120 Hz and over an energy range of 0.8 to 8 keV. FELs such as the LCLS are ideally suited for exploring entirely different problems from those outlined in Section 2, i.e., primarily those exploring the science of ultrafast phenomena and the interaction of very high intensity X-ray pulses with matter where the intensity is sufficient to reveal nonlinear interactions or even destroy the material.

FELs as currently envisaged have substantial drawbacks for the science applications emphasized here:

- Although the time average brightness is somewhat higher than can be achieved with a storage ring, it comes in very infrequent, very intense pulses that will either destroy or significantly perturb a great number of the samples described in Section 2.
- The photon energy is not easily or rapidly tunable, especially if one needs multiple, independently tunable beamlines that can simultaneously serve experiments with photons ranging from the VUV (< 100 eV) to the hard X-ray (100 keV).
- FELs may not possess the intensity, energy, and positional stability that many of the experiments outlined here demand.
- FELs typically serve one, or at most a few, beamlines and are not expected to be able to host a user community the size of the present NSLS, which numbers in the thousands.

For these reasons, there is a consensus in the community that FELs will complement rather than replace storage rings and are not an optimal choice to serve the vast majority of the science applications described in Section 2.

3.2.2 Energy Recovery Linacs

There are three particularly important time scales that characterize the behavior of the electrons in a storage ring. The revolution time is the time to complete one orbit, and is typically of order 1 μsec. As the electrons circulate, they undergo photon emission, suffer gas collisions, interact among themselves and with the vacuum chamber, etc. The small amount of energy they lose from synchrotron radiation is replenished by RF cavities; however their spatial and angular distributions are degraded by these processes. As a result, after 10^3 to 10^4 orbits, or a time scale of typically 1 to 10 msec, they evolve away from their initial injected phase space into an equilibrium one that is determined by the electron optics of the magnetic lattice. As they continue to circulate, residual gas collisions and other events kick the electrons out of the dynamic, physical, or momentum apertures and they are lost. The rate at which the

stored charge is lost determines the third fundamental time scale, i.e., the lifetime of the stored charge. All existing storage rings have been designed to achieve lifetimes of typically 10 to 20 hours.

An energy recovery linac (ERL) takes a completely new approach to generating synchrotron radiation. It is based on the assumption that one can generate the initial injected electrons with a much smaller emittance than the best equilibrium emittance that can be achieved in a storage ring, and this small emittance can be preserved while the electrons are accelerated in a linear accelerator. The injected electrons are then circulated only once before being thrown away and replaced by a fresh bunch of electrons. Since the circulating electrons are not stored, they do not live long enough to suffer the degradations in beam quality mentioned above. Thus, in principle, this concept has the potential to provide higher brightness than a storage ring. In addition, since the shape of the injected electrons might be easily controlled by a photo-injector, it could be possible to create symmetric (i.e., round) beams as opposed to the very flat beams characteristic of equilibrium in a storage ring, where the vertical emittance is typically 0.1 to 1.0 % of the horizontal emittance. Control of the initial electron bunch duration might also enable photon pulses as short as 100 fsec.

One difficulty with this approach is the energy required to accelerate fresh bunches of electrons equivalent to a current of say 500 mA to an energy of say 3 GeV, which would be 1.5 GW! This is clearly impractical, and requires that the energy of each bunch must be recovered and reused to accelerate succeeding bunches. In its most basic form then, an ERL consists of a very high quality electron source, a linear accelerator, and a magnetic lattice that contains photon radiators and returns the electron beam to the linac, as shown in Figure 3.2.1. The returned electrons enter the linac with a 180^{o} phase shift, whereby they are decelerated, returning their energy to the electric field stored in the linac, before being dumped. In this way, the ERL works on the principle of storing energy (in the linac) rather than storing charge (in the magnetic lattice).

Variations on this basic approach are also possible: N-passes through the same linac coupled with N-arcs can reduce the size of the linac and yield N different energy beams but this requires the linac to support N-times the current in one arc; linac sections can occur on opposite sides of the arc to generate two different energy beams, etc.

Since in many respects an ERL and a storage ring are very similar, an ERL would also be an essentially continuous photon source (as opposed to the slow pulsed nature of an FEL), would have broad spectral coverage, and would permit many beamlines, each easily and independently tunable in energy. The potential performance of an ERL based light source might exceed that of a storage ring with:

- average brightness as high as 10^{22} ph/sec/0.1%bw/mm^2/mrad^2
- diffraction limited round electron beams ($\varepsilon_x = \varepsilon_y$) from photo-injectors
- reduced electron energy spread giving higher brightness from long undulators and high harmonics
- very long insertion devices in the return arcs
- bunch compression to provide sub-picosecond electron bunches
- variable pulse formats for timing experiments

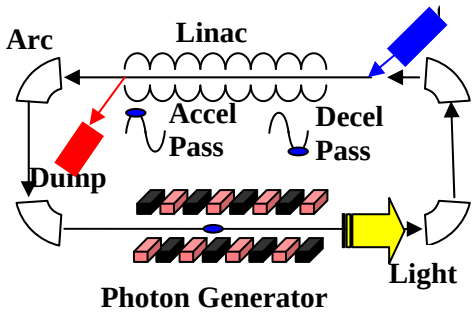

Figure 3.2.1 *Schematic illustration of the major elements of a single turn ERL light source.*

While these capabilities are attractive, there are many very formidable technological challenges that must be overcome before a light source based on this principle can be demonstrated. Chief among these is the photo-injector. The world's best photo-injectors have been developed here at BNL and are capable of producing bunches with the required emittance but only operate at ~ 10 Hz rather than the GHz rates necessary for an ERL. To put the magnitude of this jump in perspective, development of a photo-injector capable of delivering similar emittance but operating at a rate of only 120 Hz is one of the chief technical challenges that must be met for the LCLS to operate. A photo-injector suitable for an ERL must operate 10,000,000 times faster than that for the LCLS. Many other challenges also exist, such as demonstration of efficient energy recovery at the high currents and energies necessary for a synchrotron light source based on an ERL and achieving beam position stability that rivals that which can be achieved in a storage ring.

Presently, the most advanced ERLs have been developed at the Thomas Jefferson National Accelerator Facility (TJNAF). The IR FEL Demo ERL is a 50 MeV ERL that has successfully demonstrated an average circulating current of 5 mA in 2000. This ERL has recently been upgraded (2003) to try to achieve 10 mA operations and it is undergoing commissioning. There are several other facilities around the world engaged in the development of similar "low energy prototype" ERLs.

While these low energy prototype ERLs are a far cry from a 3 GeV-500 mA facility, TJNAF has taken another important step forward in ERL development by operating the CEBAF multi-turn accelerator in an energy recovery mode. A beam current of 80 μA was successfully accelerated to 1 GeV and energy recovered at 56 MeV. This is the highest energy ERL demonstrated thus far, albeit with a circulating current far below what is available in electron storage rings. What remains is to demonstrate a high average current and high energy ERL.

While a light source based on ERL technology might some day be feasible, there are many technological challenges that must first be overcome. A list of the key R&D issues is as follows:

- development of high average current (at least ~ 100 mA), low emittance electron photoinjectors (at least ~ 1 μm normalized emittance or lower)
- robust laser systems and long lifetime, high quantum efficiency, photocathode materials for photoinjectors
- demonstration of high gradient superconducting RF cavities operating in high current mode
- extraction of the higher order mode power excited by the sub-picosecond electron bunches in the superconducting linac
- beam dynamics issues such as coherent synchrotron radiation that arise for short electron bunches
- feedback systems to suppress multibunch beam breakup instabilities
- control of the electron beam halo
- positional stability of the e-beam for all beamlines
- safety systems to detect and prevent beam loss

A thorough investigation and resolution of these key R&D issues is required before the conceptual design of a high energy (E ~ 3 to 6 GeV), high average current (I ~ 100 mA or more) ERL user facility can be initiated and its eventual construction and operation assured of success.

While there are some promising indications that these challenges may one day be overcome, it is not unreasonable to expect that 10 years or more of R&D will be necessary before the feasibility of this approach can be ascertained. The need to dramatically upgrade the capabilities of the NSLS to serve the science needs outlined in Section 2 and the large northeastern research community is urgent. The opportunity cost of waiting until we know whether ERL technology will be feasible is prohibitive. A light source based on ERL technology does not meet the pressing needs outlined in this proposal.

3.2.3 Third Generation Storage Rings

Third generation storage rings are distinguished by having many cells to obtain very low emittances and many straight sections to host insertion devices. Together these result in the ability to produce very high brightness photons. Since storage rings are based on mature technology they are an excellent basis for an early project start. At the same time, there have been continued advances in key technologies whereby an advanced design can exceed the performance of existing third generation storage rings substantially. In this section, we summarize the characteristics and performance of existing third generation storage rings throughout the world as well as that of those that are not yet operational but are either under construction or in an advanced development phase.

Currently there are a total of about 50 synchrotron storage rings in operation around the world. Of these, 10 are currently operating as dedicated third generation light sources. Another 12 are either under construction or in varying stages of design. The key characteristics of these 22 machines are shown in Table 3.2.1. Only 3 are high energy machines: Spring-8 in Japan, APS in the U.S., and ESRF in Europe. To achieve high brightness, the high energy machines must have a large circumference, as shown in the table. This makes them quite expensive. The real forte of high energy machines is their ability to produce high brightness X-rays at energies above 20 keV. While there are a handful of problems that require such high energies, the majority of problems studied with synchrotron radiation do not. In addition, high

Name	**E [GeV]**	**Circum [m]**	**Current [mA]**	**Emittance [nm-rad]**	**Cells (i.e., Straights)**	**Lattice**	**Full Energy Injection**	**Year Commis-sioned**
SPRING-8	8	1436	100	5.6	48	DBA	Y/Booster	1997
APS	7	1060	100	3.5	40	DBA	Y/Booster	1995
ESRF	6	844	200	3.8	32	DBA	Y/Booster	1994
PLS	2.5	281	180	12	12	TBA	Y/Linac	1995
ANKA	2.5	240	110	70	8	DBA	N/μtron	2000
SLS	2.4	240	400	5	12	TBA	Y/Booster	2001
ELETTRA	2-2.4	260	320	7	12	DBA	N/Linac	1993
NANO-HANA	2	102	300	70	8	DBA	N/Booster	2004
ALS	1.9	197	400	6.8	12	TBA	N/Booster	1993
BESSY-II	1.7-1.9	240	270	5.2	16	DBA	Y/Booster	1998
SPEAR3	3	240	500	18	18	DBA	Y/Booster	2004
CLS	2.9	171	500	18	12	DBA	Y/Booster	2003
SOLEIL	2.85	354	500	3.1	16 + 8	DBA	Y/Booster	2005
DIAMOND	3	560	300	2.7	24	DBA	Y/Booster	2006
AUST. SYNCH.	3	216	200	8.6	14	DBA	Y/Booster	2007
LLS	2.5	252	250	8.5	12	TBA	Y/Booster	?
SSRF	3.5	396	300	4.8	20	DBA	Y/Booster	?
MAX-IV	3	285	500	1.2	12	7BA	Y/?	?
SESAME	2.5	120	400	27	16	DBA	N/Booster	2008
TLS-II	3	240	400	10	16	DBA	N/Booster	?
CANDLE	3	224	350	8.4	16	DBA	Y/Booster	?
INDUS-II	2.5	173	300	58	8	DBA	N/Booster	?

Table 3.2.1 *Key characteristics of third generation light sources around the world. Top group: Existing dedicated machines which were commissioned after 1990, by decreasing order of electron energy. Bottom group: New machines at various stages of construction or development. If a commitment to build the machine has not yet been made, or the commissioning date is uncertain, year commissioned is shown as a question mark.*

energy machines are not optimal for producing bright photons in the VUV and soft X-ray energy range. In light of these factors, it is generally viewed as sufficient that each of the major scientific continents have one high energy third generation light source and there are currently no plans anywhere to build another high energy machine.

The 19 remaining machines in Table 3.2.1 are so-called medium energy machines, having energies ranging from 1.7 to 3.5 GeV. Brightness and flux are two of the most important figures of merit for a light source. The electron emittance is proportional to the square of the electron energy, making brightness inversely proportional to the fourth power of the electron energy. The total power of radiation from an undulator at any given photon energy is directly proportional to the current times the square of the electron energy and the power density is proportional to the current times the fourth power of the electron energy. Thus, lowering the storage ring energy can raise the brightness and increase the flux by permitting lower emittance and higher current. Countering this is the fact that the undulator photon energy is proportional to the electron energy squared and producing high energy photons from a medium energy storage ring requires shorter period undulators. However, there have been tremendous advances in undulator technology, leading to short period undulators capable of producing hard X-rays from medium electron energies. Even greater advances are expected in the near future with the development of superconducting undulators. As a result, medium energy third generation storage rings meet or exceed the performance of the high energy machines in the most desired energy range of 0.3 to 20 keV at a significantly lower cost.

The most advanced medium energy machine under construction is the Diamond light source, scheduled to be commissioned in 2006. As indicated in Table 3.2.1, Diamond will have the lowest emittance (2.7 nm) of any existing storage ring when it begins operations in 2007. NSLS-II will go beyond this value to 1.5 nm. Of course, emittance is only one metric of storage ring performance. To most users, the brightness, flux, and stability are of more immediate relevance to the quality of science the facility can support. More detailed comparisons are made between the expected performance of NSLS-II and other facilities in Section 3.3.

3.3 NSLS-II: An Advanced Medium Energy Storage Ring

It is clear from the above discussion that only a third generation storage ring can meet the urgent needs of the large user community who demand very high average brightness and flux in the VUV, soft, and hard X-ray energy regions, together with exquisite intensity, position, and energy stability, which are required to enable the scientific opportunities described in Section 2. The centerpiece of the new NSLS-II facility will be an advanced, highly optimized medium energy third generation storage ring. It will take advantage of the latest advances in storage ring technology, including superconducting undulators, top-off operation, superconducting RF cavities, and others, to achieve world-leading average brightness and flux in the target spectral region from 10 eV to 20 keV and set a new performance standard. It will be designed to be upgradeable to operation as an energy recovery linac for even greater performance, should that technology become feasible in the future. Relocating the present VUV/IR storage ring to the new facility to serve as a dedicated IR ring is a cost effective way to also provide world-leading high brightness in the important near- to far-IR spectral region. The IR ring will offer even better performance than the current VUV/IR ring in the IR region by operating in top-off mode using the first 800 meV of the same linac used to perform top-off injection of the X-ray ring.

A detailed conceptual design of the new X-ray ring will be initiated upon approval of this proposal. However, we have already done sufficient analysis to determine the major elements of NSLS-II and its anticipated performance:

- Ultrahigh brightness (~10^{21} ph/sec/0.1%bw/mm^2/mrad^2)
- Ultrahigh flux (~10^{16} ph/sec/0.1%bw)
- Electron energy of 3.0 GeV
- Circumference in the range of 600 to 700 m
- Ultra-low emittance (horizontal ~ 1 nm; vertical ~ 10 pm, which is diffraction limited at 1 Å)
- Very high stored current of at least 500 mA
- Top-off operation with a full energy injector
- Superconducting small gap undulators for continuous tunability
- Large number of insertion devices (> 20)
- Potential to be upgraded in the future to operation as an energy recovery linac

Obtaining this level of performance will be challenging. The design considerations and issues that must be overcome to meet these goals are discussed in detail in Section 3.4. Based on those considerations, we have done a preliminary conceptual and engineering design as well as a cost estimate for a 620 m circumference 3 GeV storage ring with a Triple Bend Achromat (TBA) lattice, 24-fold symmetry, and 7 m straight sections. The storage ring is housed in a building that allows room on the experimental floor for all beamlines to extend 60 m from the source to the end of the beamline. The shield wall is 25 m from the source, so a beamline length of 60 m was chosen to accommodate 1:1 imaging of the beam on the sample. While this is expected to be sufficient for the majority of cases, there may be a few special needs for extra long beamlines, for example for coherence experiments. As discussed in Section 3.6, the siting of the facility has been chosen to allow for longer beamlines to be built as extensions coming out of the building, as needed.

Figure 3.3.1 shows a computer rendering of the exterior of the facility and Figure 3.3.2 shows a schematic drawing of major elements of the facility. Table 3.3.1 lists the initial parameters of the design. The injection system will be either a full energy linac or a full energy booster sufficient to operate the storage ring in top-off mode. Figures 3.3.1 and 3.3.2 show a full energy linac. The gross square feet associated with the various elements shown in Figure 3.3.2 are given in Table 3.3.2. Figure 3.4.5 later in the text shows an alternative booster injection system. The new facility will be situated directly across from the current NSLS building and the new Brookhaven Center for Functional Nanomaterials.

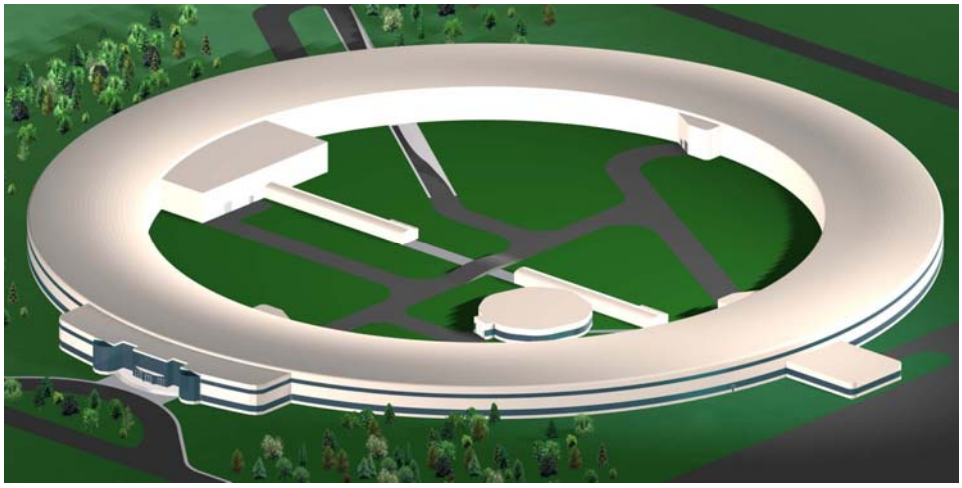

Figure 3.3.1 *Computer rendering of the exterior of the NSLS-II storage ring. The main entrance is shown to the lower left, the RF gun chamber is to the lower right outside the ring, and the buildings housing the klystron galleries for the linac injection system (which is itself below ground), are shown in the infield of the ring. The small circular building in the infield is the IR ring, which shares the first portion of the same injection system used to top-off the X-ray ring.*

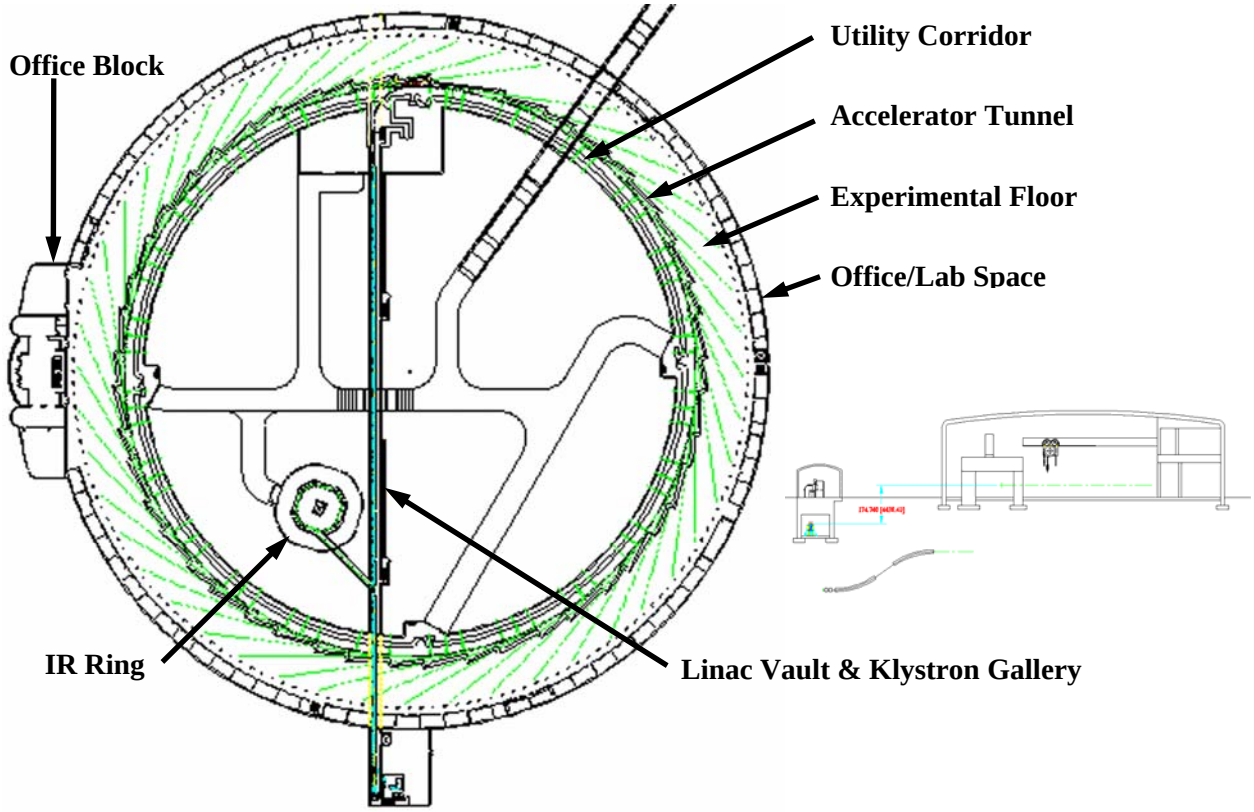

Figure 3.3.2 *Schematic of NSLS-II facility, showing the full energy linac injection system (blue) injecting first the small IR ring and then the much larger X-ray ring, the beamlines (in green) and surrounding lab/office space. A cross-sectional view on the right shows, in order from left to right, the linac tunnel and klystron gallery, utility corridor, accelerator tunnel, experimental floor, and perimeter lab/office space.*

NSLS-II Parameters	
Circumference	620 m
Energy	3.0 GeV
Current	500 mA
Emittance (ε_x, ε_y)	1.5, 0.008 nm
Beam Size (σ_x, σ_y)	84.6, 4.3 μm
Beam Divergence (σ_x', σ_y')	18.2, 1.8 μrad
Pulse Length (rms)	11 psec

Table 3.3.1 *Main parameters for NSLS-II.*

Building Area	**Area [SF]**		
	First Floor	Second Floor	Total
Linac Vault & Klystron Gallery	12,493	6,068	18,561
Utility Corridor	14,578		14,578
Accelerator Tunnel	51,563		51,563
Experimental Floor	111,230		111,230
Office/Lab	64,173	64,173	128,346
Office Block	11,055	8,945	20,000
TOTAL	**265,092**	**79,186**	**344,278**

Table 3.3.2 *Gross square feet associated with conventional construction for NSLS-II. The different building areas are indicated in Figure 3.3.2.*

The X-ray storage ring will more than double the number of insertion device beamlines to 21 compared to the combined total of 9 once the remaining straights are built out on the current X-ray and VUV/IR ring (see Table 3.1.2) One straight section is reserved for injection and two are reserved for superconducting RF cavities and a third harmonic RF stretcher cavity. Most of the insertion devices will be superconducting undulators to provide fully tunable radiation from this medium energy ring. More information on insertion devices is given in Section 3.4.12.

Fig. 3.3.3 gives the average brightness and flux of the insertion devices and bending magnets on the NSLS-II X-ray storage ring, and compares them to those on the present X-ray ring and VUV/IR ring. NSLS-II undulators will be more than 10,000 times brighter than the present brightest NSLS beamline, X25, in the hard X-ray region above ~ 3 keV. In the soft X-ray region from ~ 200 eV to ~ 3 keV, NSLS-II soft X-ray undulators will be 1,000 times brighter than the present brightest NSLS beamline, X1. And in the UV and VUV region from 10 to 200 eV, NSLS-II undulators will be 100-1,000 times brighter than the brightest VUV undulator, U5, on the present VUV/IR ring. The flux from the undulators will also increase substantially, especially in the soft and hard X-ray energy regions, where there will be ~ 20 times greater flux from ~ 200 eV to ~ 60 keV. The 24 bending magnet beamlines will have more than 100 times higher brightness and several times higher flux than the present NSLS bending magnet beamlines throughout the entire energy range from 10 eV to more than 60 keV.

The brightness and flux of the NSLS-II X-ray storage ring will also be significantly greater than that of any other storage ring in the US or abroad. Figure 3.3.4 compares the brightness and flux of NSLS-II to that of other leading synchrotrons around the world, including the present Advanced Photon Source (APS), Advanced Light Source (ALS), and European Synchrotron Radiation Facility (ESRF). NSLS-II will be 10-100 times brighter than these facilities from ~ 2 keV to > 20 keV and from 10-1000 times brighter from 10 eV to 2 keV. The flux from NSLS-II undulators will be 1.5-100 times higher than from these other machines throughout the energy range from 10 eV to > 20 keV.

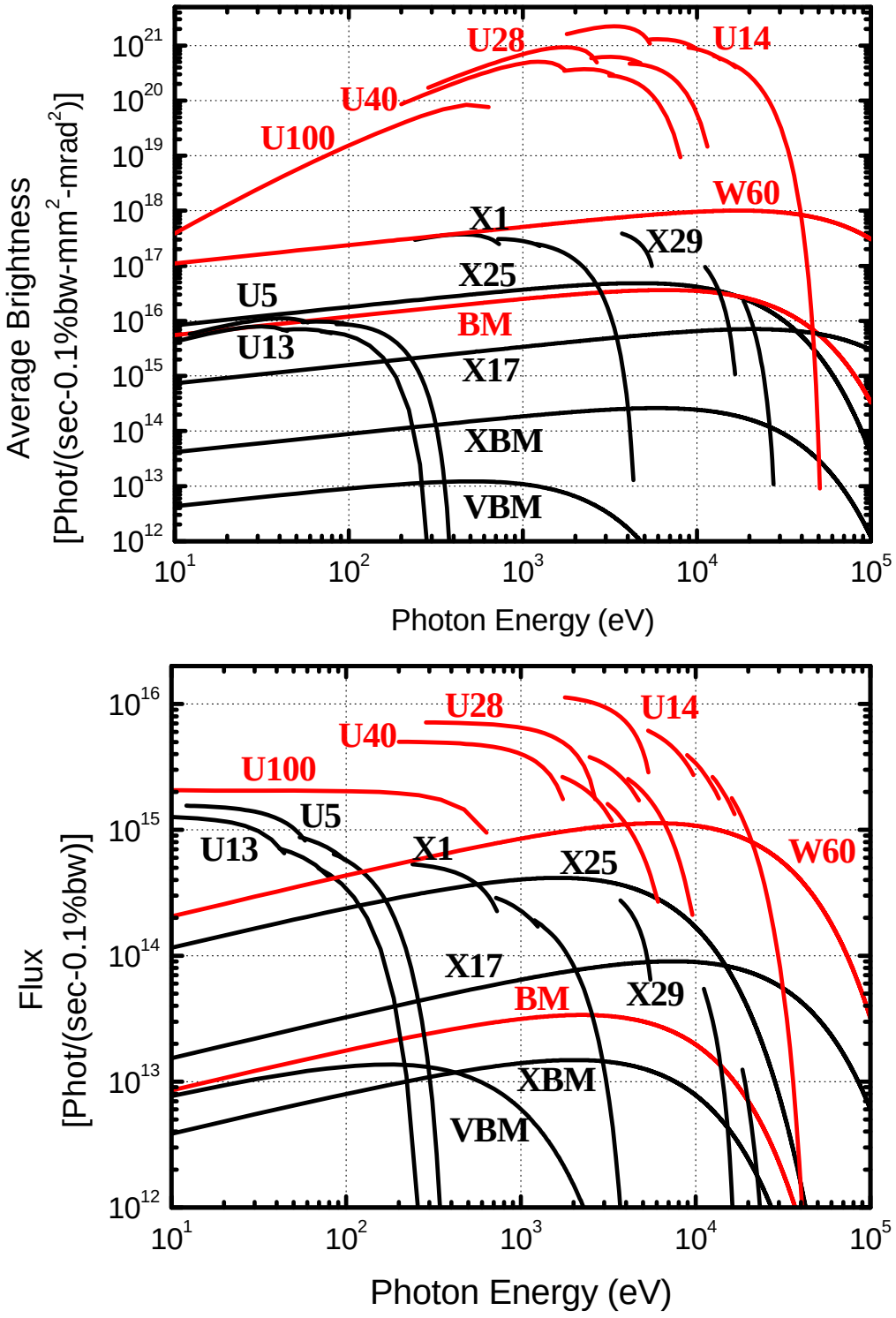

Figure 3.3.3 *Average brightness (top) and flux (bottom) of insertion devices and bending magnets on NSLS-II (red) compared to the existing NSLS (black). U = Undulators, W = Wiggler, BM = Bending Magnet. The parameters of the NSLS-II undulators and wiggler are given in Section 3.4.12.*

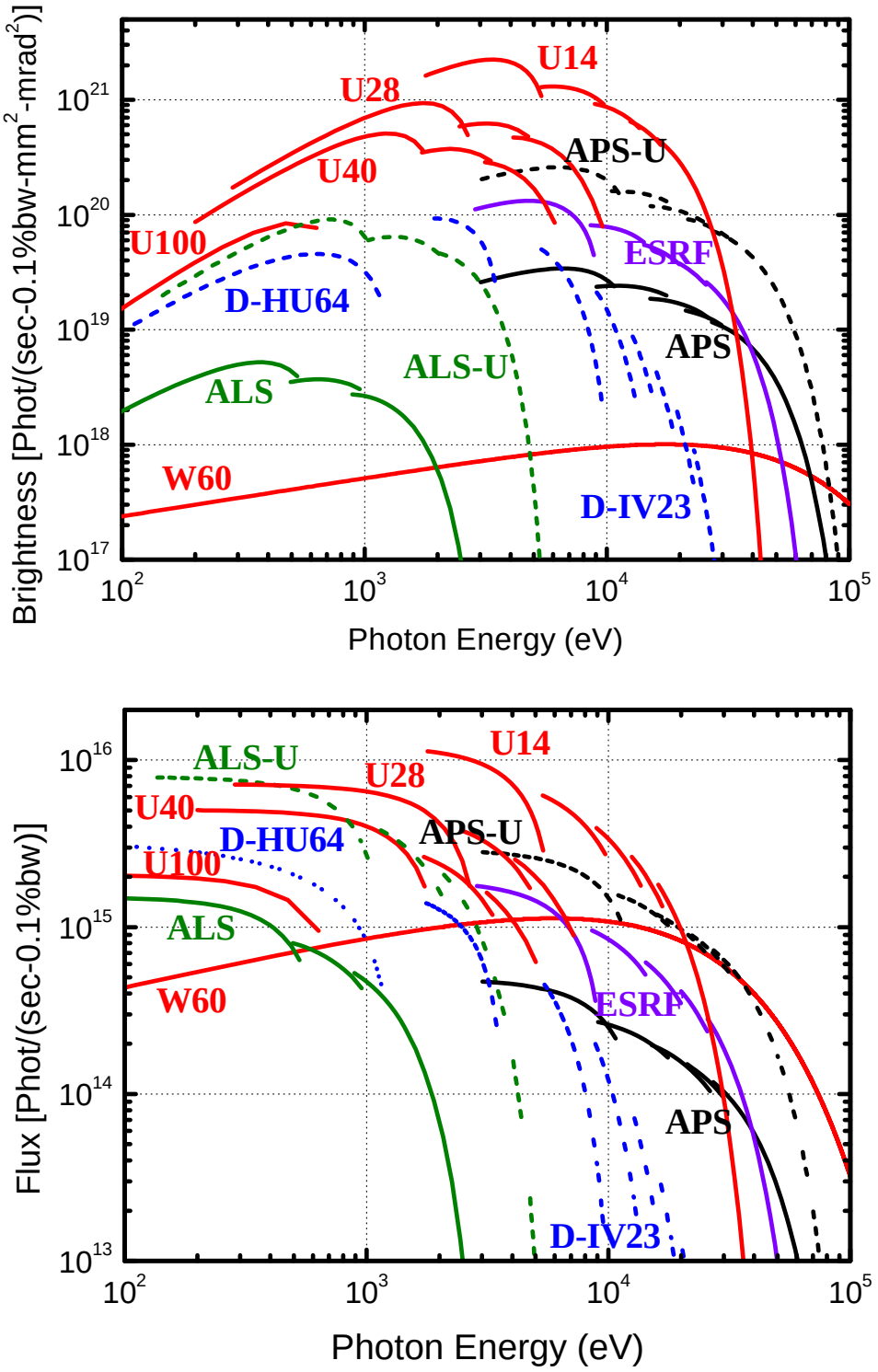

Figure 3.3.4 *Average brightness (top) and flux (bottom) of insertion devices at NSLS-II compared to devices at APS, ALS, ESRF, and Diamond (which is expected to be operational in 2007). The performance of proposed upgrades of APS [1] and ALS [1, 2] are also shown for comparison. The performance of NSLS-II will be world leading in both brightness and flux*

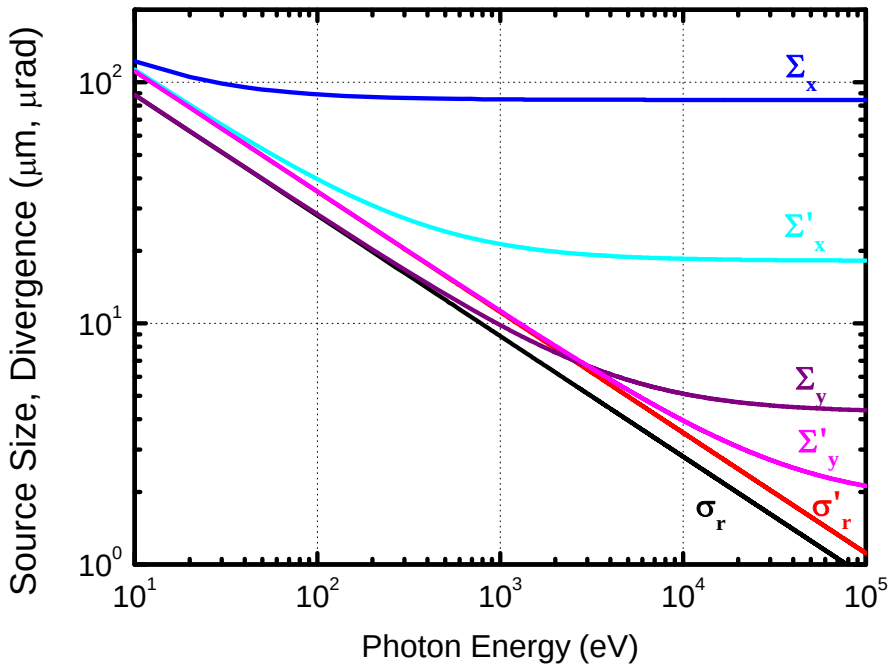

Figure 3.3.5 *Photon beam source sizes, $\Sigma_{x,y}$, and divergences, $\Sigma'_{x,y}$, for radiation emitted from a 5 m long undulator at NSLS-II compared to the natural, diffraction limited, photon source size, σ_r, and divergence, σ'_r. This shows that the photon beam size and divergence will be essentially diffraction limited in the vertical, and have a high degree of coherence in the horizontal, at photon energies of ~ 10 keV and below.*

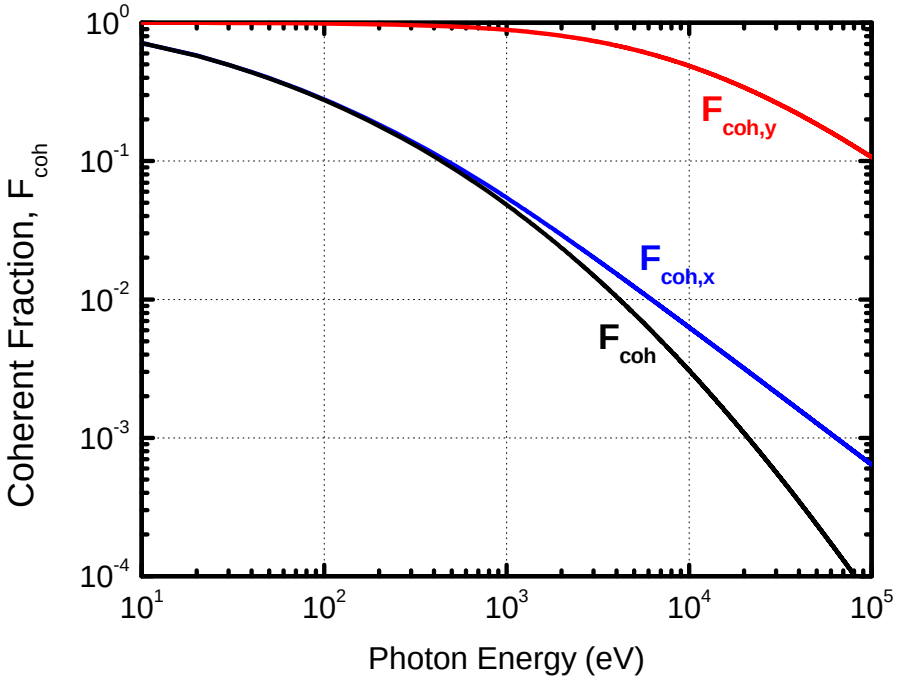

Figure 3.3.6 *Vertical, horizontal, and overall coherent fraction for photons emitted by 5 m long undulators at NSLS-II. This shows the nearly diffraction limited quality of the photons in the vertical, and high coherence in the horizontal, at photon energies of ~ 10 keV and below.*

As discussed in Section 3.4.1, the very low emittance of the electron beam in the NSLS-II X-ray ring results in very small photon beam source sizes and divergences and a high degree of coherence of the radiated photons, especially in the vertical direction. These photon properties are crucial for many of the most challenging problems described in Section 2. Figure 3.3.5 shows the effective source size and divergence of photons emitted by a 5 m long undulator as a function of energy from 10 eV to 100 keV and Figure 3.3.6 shows the corresponding coherence fraction (defined in Section 3.4.1) in the vertical and horizontal directions, as well as the overall coherence fraction. These curves show that the radiation from NSLS-II will be essentially diffraction limited in the vertical direction below about 10 keV and have a high degree of transverse coherence in the horizontal direction.

NSLS-II will continue to be world-leading in brightness and flux for many years after it begins operations in 2012. Among future machines listed Table 3.2.1, the Diamond facility is among the most advanced. As shown in Figure 3.3.4, NSLS-II will significantly surpass the performance of Diamond in both brightness and flux throughout the spectral range. In addition to future new machines, there may also be future upgrades of existing machines. Upgrades of both the APS [1] and the ALS [1, 2] have been proposed. The expected performance if those upgrades do take place is also shown in Figure 3.3.4. Again, NSLS-II significantly exceeds the performance of both the ALS and APS upgrades throughout the spectral range. Thus, we conclude that NSLS-II will continue to be a world-leading synchrotron in both brightness and flux for many years after it becomes operational.

As mentioned above, the existing VUV/IR ring will be relocated to the new facility to serve as a dedicated IR ring and support science at near- to far-IR photon energies. The ring will be upgraded to have a 500 MHz RF system to enable it to share the NSLS-II injection system. The first 800 meV of the linac injector will serve as a full energy injector for the IR ring, allowing it to run in top-off mode with 1000 mA stored current. This high stored current plus the very large opening angles (90 mrad^2) possible

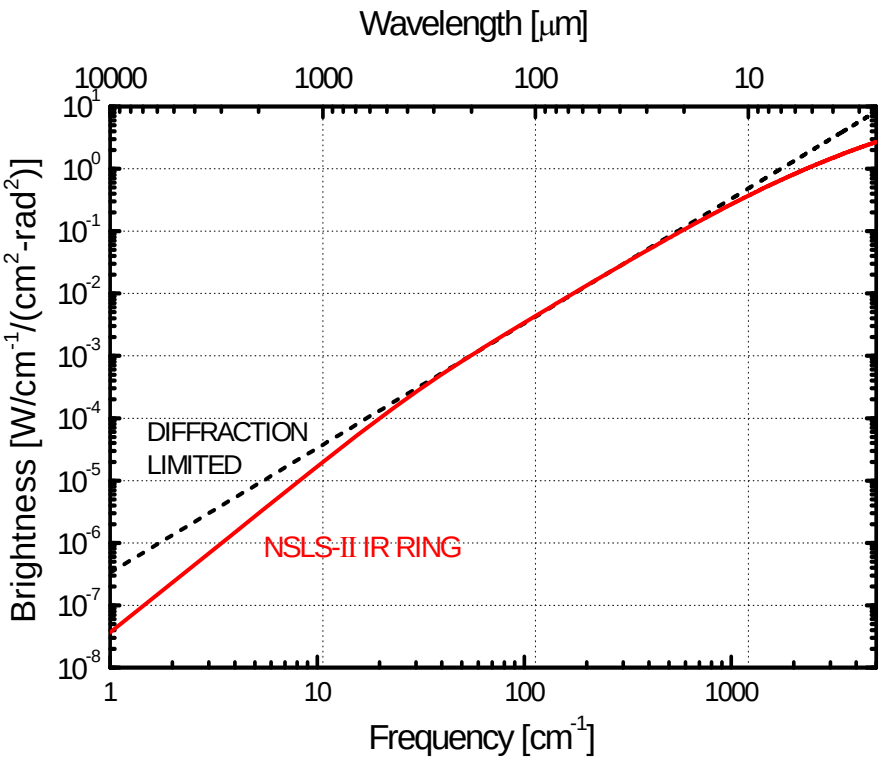

Figure 3.3.7 *Calculated brightness for the NSLS-II IR ring at 1000 mA and a 90 x 90 mrad^2 extraction aperture, compared to the brightness of an ideal diffraction limited source at 1000 mA. The NSLS-II IR ring will have world-leading brightness and be at or near the diffraction limit throughout the near- to far-IR spectral region.*

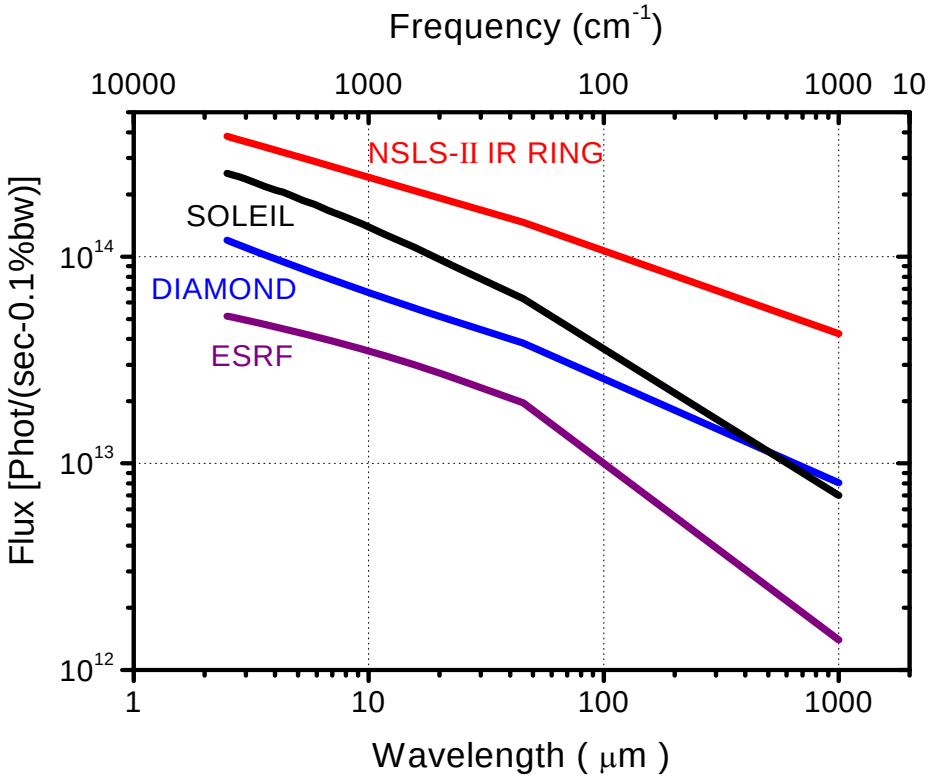

Figure 3.3.8 *Photon flux in the infrared of the NSLS-II IR ring compared with typical 3rd generation synchrotron sources. The high stored current and large opening angles (90 mrad^2) possible on the NSLS-II IR ring result in world leading IR flux and brightness.*

on the IR ring will result in world leading brightness throughout the IR spectral region, as shown in Figures 3.3.7 and 3.3.8. The upgraded higher frequency RF system will also result in significantly shorter (10s of picoseconds) electron bunches than the current VUV/IR ring, benefiting the time-resolved spectroscopy program. The high RF frequency also creates exciting possibilities for producing super-radiant THz radiation [3], which will be explored further during development of the Conceptual Design.

REFERENCES

[1] http://www.sc.doe.gov/bes/besac/20yearagenda.pdf and unpublished. APS has proposed a 4 stage upgrade. The performance improvements resulting from stages I and II were used as a basis for calculating the upgraded APS performance shown in Figure 3.3.4.

[2] http://www-als.lbl.gov/als/20/ALStext.html

[3] M. Abo-Bakr, J. Feikes, K. Holldack, P. Kuske, W.B. Peatman, U. Schade, and G. Wüstefeld, H.-W. Hübers, Phys. Rev. Lett. 90, 094801-1 (2003).

3.4 Design Considerations and Challenges

The main figures of merit for NSLS-II and their primary determinant factors are:

- *High Brightness*: Current, number of undulator periods, electron beam emittance
- *High Flux*: Current, number of undulator periods
- *Photon Spectrum*: Electron energy, period of undulators
- *Beam Quality*: Position, energy, and intensity stability, reliability, Mean Time Between Failures

To maximize these figures of merit, NSLS-II should have the highest possible stored current, long straight sections for a large number of undulator periods, the lowest possible electron emittance, and well chosen electron energy, while at the same time achieving record setting stability and reliability at a reasonable cost. These are the same requirements confronted in the design of any modern synchrotron and as we discuss, many of them are contradictory. By taking advantage of the experience of current synchrotrons and also of recent and forthcoming technological advances, we believe that NSLS-II will out-perform any other medium energy synchrotron. In this section, the design considerations, initial choices, and future challenges encountered in achieving these ambitious goals are discussed in detail.

3.4.1 Introduction

We begin by reviewing the factors that determine the brightness from undulator insertion device sources in an electron storage ring. When an electron traverses an undulator insertion device in the z direction, with a periodic magnetic field $\vec{B} = B_u \cos(k_u z)\,\vec{y}$ in the y direction, it undulates in the horizontal plane (x direction) as shown in Figure 3.4.1. The undulator is characterized by its period, λ_u, and its strength parameter, $K \equiv (eB_u\lambda_u)/(2\pi mc)$.

The accelerated electron emits radiation at odd harmonics of the fundamental undulator period but reduced in wavelength by the relativistic factor of $2\gamma^2$, where γ = 1957 E [GeV]. The wavelength of radiation emitted in the forward direction is

$$\lambda_n = \frac{\lambda_u}{2n\gamma^2}\left(1 + K^2/2\right), \qquad n = 1, 3, 5, \ldots,$$

The central cone flux of the radiated photons, Φ, is proportional to the number of periods of the undulator, N_u, and the stored electron current, I,

$$\Phi \sim N_u I$$

The on axis brightness (sometimes also referred to as brilliance), B, of the radiated photons is defined

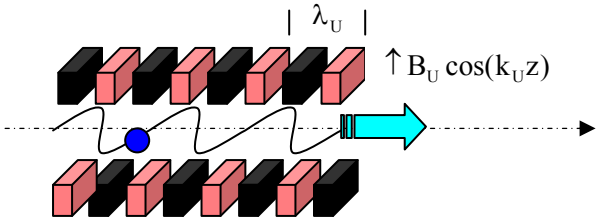

Figure 3.4.1 *Schematic illustration of an electron radiating in an undulator.*

as Φ divided by the phase space area of the source, which is determined by the horizontal and vertical photon beam source sizes, $\Sigma_{x,y}$, and divergences, $\Sigma'_{x,y}$,

$$B = \frac{\Phi}{4\pi^2 \Sigma_x \Sigma'_x \Sigma_y \Sigma'_y}$$

Both the electron beam source sizes, $\sigma_{x,y}$, and divergences, $\sigma'_{x,y}$, as well as the natural (diffraction limited) photon source size, σ_r, and divergence, σ'_r, for photons emitted by an undulator of length L contribute to $\Sigma_{x,y}$ and $\Sigma'_{x,y}$,

$$\Sigma_{x,y} \equiv \sqrt{\sigma_{x,y}^2 + \sigma_r^2} \qquad \Sigma'_{x,y} \equiv \sqrt{\sigma'^2_{x,y} + \sigma'^2_r}$$

where

$$\sigma_x = \sqrt{\varepsilon_x \beta_x + \sigma_\varepsilon^2 \eta_x^2} \qquad \sigma'_x = \sqrt{\varepsilon_x \gamma_x + \sigma_\varepsilon^2 \eta'^2_x},$$

$$\sigma_y = \sqrt{\varepsilon_y \beta_y} \qquad \sigma'_y = \sqrt{\varepsilon_y \gamma_y},$$

$$\sigma_r = \sqrt{\lambda 2L}/(4\pi) \qquad \sigma'_r = \sqrt{\lambda / 2L},$$

Here $\gamma_{x,y} \equiv (1+\alpha_{x,y}^2)/\beta_{x,y}$, $\alpha_{x,y} \equiv -\beta'_{x,y}/2$, $\varepsilon_x \equiv \varepsilon/(1+\chi)$, $\varepsilon_y \equiv \chi\varepsilon/(1+\chi)$, and β, χ, σ_E and $\eta_{x,y}$ are the betatron functions, vertical emittance coupling, electron energy spread, and energy dispersion factors, respectively.

The peak brightness is simply the brightness per pulse,

$$B_p = \frac{B}{f\,\tau}$$

where f is the number of electron bunches per second and $\tau = 2.35\sigma_\tau$ is the FHWM pulse length (σ_τ is the rms pulse length).

Another important figure of merit is the flux of photons that are transversely coherent, Φ_c. This is given by

$$\Phi_c = B\left(\frac{\lambda}{2}\right)^2$$

The fraction of photons that are transversely coherent, F_c, is given by

$$F_c = \frac{\Phi_c}{\Phi} = \frac{\lambda^2}{(4\pi)^2 \Sigma_x \Sigma'_x \Sigma_y \Sigma'_y}$$

Since $\Sigma_{x,y}$ and $\Sigma'_{x,y}$ include the contributions of the electron and the photon emittances, the coherent fraction, F_c, only approaches unity when the electron emittance is much smaller than the photon emittance.

The design of the magnetic lattice of the storage ring determines ε, α, β, χ, σ_E and $\eta_{x,y}$. Since the goal in designing NSLS-II is to produce high brightness photon beams, we want to make the electron emittance, ε, be small compared to the natural photon emittance, $\varepsilon_r = \sigma_r\sigma_r' = \lambda/(4\pi)$. Thus, for diffraction limited X-rays at an energy of 12 keV ($\lambda \sim 1$ Å), the electron emittance, ε, should be ~ 8 picometer.

The very low horizontal emittance of NSLS-II of ~ 1.5 nm, together with vertical emittance coupling, χ, of 0.5%, means that the vertical emittance will, in fact, be ~ 8 picometer. Thus, the radiation in the vertical direction should be essentially diffraction limited below ~ 12 keV, which is indeed the case, as shown in Figures 3.3.5 and 3.3.6.

3.4.2 Lattice

The equilibrium emittance in an electron storage ring results from a balance between the quantum excitation of the electron beam during the emission of radiation in the dipole magnets and the damping of these oscillations by the acceleration in the RF system. For a ring made up of isomagnetic dipole magnets, the horizontal emittance, ε, of the electron beam can be written as

$$\varepsilon = F\frac{\gamma^2\theta_d^3}{J_x},$$

where F depends on the choice of lattice and how it is tuned, and θ_d and J_x are the bend angle of the dipole magnets and the horizontal damping partition function, respectively. The dependence on γ^2 shows why it is harder to make a low emittance storage ring as the electron energy increases.

The basic approach to constructing a low emittance light source is thus to use a large number of short magnets (small θ_d), make a wise choice of the lattice type and tuning to minimize F, and increase the value of J_x with combined function dipoles if needed (in which case J_x increases from 1 to 2). In general, a light source lattice is constructed from 'basic cells', containing dipoles, quadrupoles and sextupoles, which are usually bounded by dispersion free drift spaces for insertion devices. Since θ_d decreases as the number of cells and the number of magnets per cell increases, the emittance is minimized by having a large number of cells and a large number of bends per cell. This tends to increase the circumference of the storage ring, which makes the cost increase. The dependence on γ^2 means this is even more necessary for a high energy storage ring and explains why SPRING-8, APS, and ESRF all have the largest circumferences in Table 3.2.1.

This also explains why it is not possible to obtain the required gains in performance simply by rebuilding the existing NSLS storage ring. Even if this were done (which would require a two to three year shutdown), it is constrained by its small (170 m) circumference to have too few cells and too few straight sections for insertion devices so that the gains would be minimal.

In our pre-conceptual design work, we have considered a 24 cell Triple Bend Achromat (TBA) with 7 m long straight sections. This is a relatively large number of cells compared to other recent synchrotrons, (see Table 3.2.1). The only exceptions are Diamond, which also has 24 cells, and the higher energy rings, SPRING-8, APS, and ESRF. Twenty-four cells is chosen to give us a smaller emittance and is also considered to be the minimum number of straight sections (i.e., insertion devices) required to serve the needs of the broad range of scientific problems described in Section 2.

A TBA lattice is chosen for three reasons. First, it gives us more magnets per cell, which, while slightly more expensive, gives us a smaller emittance for a given circumference. This is again in contrast to the choice most synchrotrons have made, which is to employ a Double Bend Achromat (DBA) lattice

(see Table 3.2.1). The exceptions are the Pohang Light Source (PLS), the Swiss Light Source (SLS), the Advanced Light Source (ALS), and the proposed Synchrotron Light Laboratory at Barcelona (LLS). All of these are relatively small circumference machines that have a relatively low emittance for their number of cells and circumference. Second, it provides the ability to tune the momentum compaction while still maintaining zero dispersion ($\eta = 0$) in the straight sections. This is a key requirement to preserve the ability to upgrade NSLS-II to operate in an ERL mode in the future (see Section 3.5.2). Third, it is much easier to add so-called 'SuperBends' to a TBA lattice. This is under consideration as an additional means of providing high energy photons from superconducting bending magnets.

The last of the basic defining parameters, the straight section length, is chosen to be a relatively long 7 m to permit long undulators (large number of periods and hence higher brightness) and to meet the needs of injecting into the ring (see Section 3.4.10).

Altogether, these basic design parameters determine the overall storage ring circumference, which, at 620 m, will be the largest medium energy storage ring in the world (see Table 3.2.1).

There are many challenges to be overcome in actually realizing such an ultra-low emittance storage ring. Achieving low emittance requires segmenting the ring into many cells with short dipoles interspersed with lots of strong quadrupoles to focus the electron beam. The strong quadrupoles contribute strong chromatic aberrations that must be corrected with nonlinear sextupole magnets and the short dipoles result in small dispersion so the sextupoles must be very strong and this makes the lattice

Lattice Type	TBA
Circumference [m]	620.4
Superperiods	24
Straight Section Length [m]	7
Energy [GeV]	3
Horizontal Emittance, ε_x [nm]	1.54
Vertical Emittance, ε_y [nm]	0.008
Emittance coupling, χ	0.5%
Momentum Compaction, α	0.0000815
Dipole Radius, ρ [m]	7.64
Bending Magnet Critical Energy [eV]	7840.6
Field Index	21.5
Betatron Tunes Q_x, Q_y	37.3 , 17.25
Uncorrected Chromaticity, ξ_x, ξ_y	-108.8 , -31.6
ID Beta Functions, β_x, β_y [m]	4.65 , 2.37
Damping Partition Functions, J_x, J_e	1.044 , 1.956
Energy Loss in Dipoles U_o [MeV/turn]	0.938
V_{rf} [MV]	1.55
RF Frequency [MHz]	500
RF Acceptance, ε_{RF} [%]	3
Current [mA]	500
Revolution frequency [kHz]	483.9
Orbit Time [μsec]	2.07
Maximum number of RF buckets	1035
Filled RF buckets (2/3 filling)	690
Single Bunch Current (2/3 filling) [mA]	0.72
Single Bunch Charge (2/3 filling) [nC]	1.48
Bunch length, σ [mm, ps]	3.3, 11
Natural Energy Spread [%]	0.094

Table 3.4.1 *Initial TBA lattice parameters for NSLS-II.*

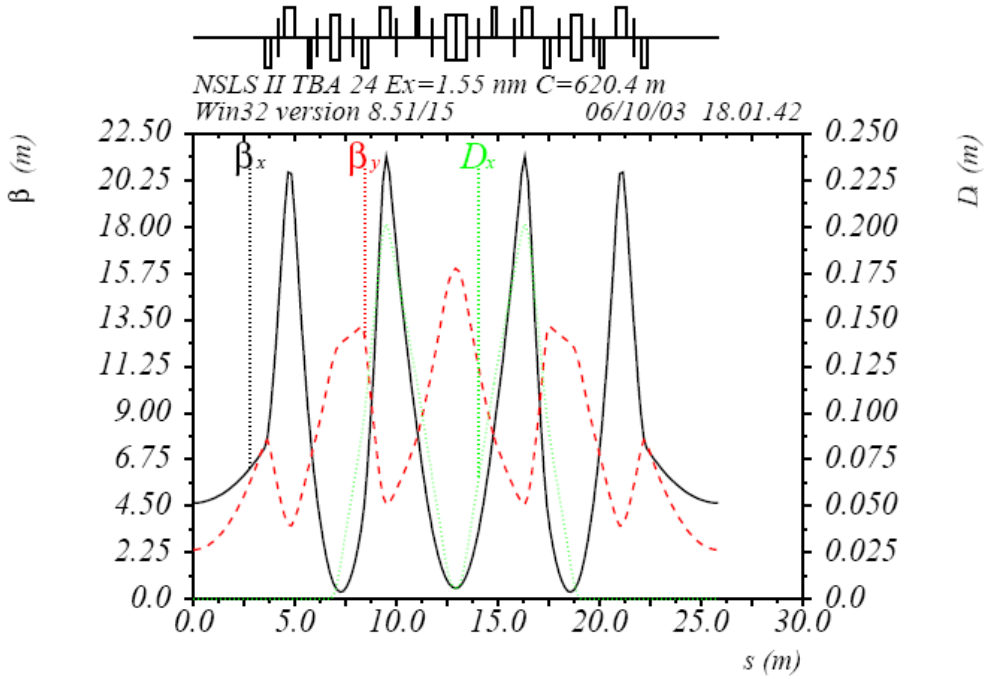

Figure 3.4.2 *Betatron and dispersion functions for one superperiod of the TBA lattice for NSLS-II.*

highly nonlinear. The resulting stable phase space available to inject the electrons into the machine and to maintain a good lifetime is compromised (i.e., the dynamic aperture is reduced).

Achieving this leads to small beams (and hence a need for *high beam stability*), low dynamic and physical aperture and low lifetime (and hence the need for a *low emittance, high rep rate injector*), and potential collective effects and instabilities (and hence *sophisticated feedback systems* to cope with them). In addition, all of this must be achieved at a reasonable cost.

The parameters for our preliminary design of the lattice are listed in Table 3.4.1 and Figure 3.4.2 displays the betatron and dispersion functions for one superperiod. Analysis is underway to determine the optimal sextupole placement to maximize the dynamic aperture. Three families of sextupoles located inside the achromats are being used to correct the chromaticity and two or more families are located outside the achromat to improve the dynamic aperture, betatron tune shift with amplitude and nonlinear chromaticity. State of the art lattice and tracking tools such as OPA, TRACY, ACCELERATOR TOOLBOX and FREQUENCY MAP ANALYSIS are being employed.

The complex task of nonlinear optimization of the storage ring lattice is in its very early stages and much work remains to be done during the development of the full conceptual design. Future tasks include determining optimum betatron tunes and straight section betatron functions; determining the optimum number of sextupole families and locations; considering lattices with reduced superperiodicity to incorporate different straight sections; performing dynamic aperture tracking, including the effects of magnet errors and insertion devices; optimization of the off energy behavior of the lattice to ensure a good Touschek lifetime and injection efficiency.

At the present stage of the machine design all of the straight sections are taken to be of equal length at 7 meters to maximize the superperiodicity and thereby optimize the dynamic aperture of the ring. As the machine design evolves we envision reducing the periodicity of the ring and incorporating perhaps four longer straight sections ~ 20 m in length. These would allow for a more optimum injection straight as well as accommodate very long large gap devices used for soft X-ray or VUV production. Longer straights would also facilitate the possible future conversion of the ring to an energy recovery linac mode of operation. Depending on the desired gap of the insertion device in the long straight section it may be necessary to segment the undulators with quadrupoles in between sections to control the growth of the

betatron functions. These issues will be explored further during development of the full conceptual design.

3.4.2.1 Lattice Magnets

In designing the lattice magnets several advantageous features will be utilized. Since the ring energy is fixed, the magnetic field will not be ramped with beam stored, so solid, rather than laminated, low-carbon steel may be used for the yokes. Attention will need to be paid to homogeneity and magnetic field uniformity of the steel. The dipoles will be open on the outside of the ring to allow synchrotron radiation from the dipoles to be brought out tangentially and so can have C-frame yokes. The quadrupoles and sextupoles may also be split into C-frames (dipoles into halves, sextupoles into thirds). Design studies will be conducted to optimize the magnet designs from the standpoint of magnetic, mechanical, thermal, and assembly considerations. The long and short dipoles can use a gradient design to provide a modest amount of vertical focusing by a radial taper in the magnet gap. Angled vertical magnet faces can also be used to provide horizontal focusing.

During development of the full conceptual design, we also plan to explore the following three design alternatives for the lattice magnets: conventional discrete electromagnets, integrated common-yoke magnet assemblies, and permanent magnet-driver dipoles.

The ring magnets may be realized with conventional, iron-core, water-cooled electromagnets. The required dipole fields, dipole gradients, quadrupole gradients, and sextupole fields are all readily achievable. The vertical stay-clear apertures, and therefore the magnet gaps, are about 40% smaller than in the present NSLS, so the required ampere-turns will be less and the resulting magnets will be more compact.

Several magnets may be integrated into a single, monolithic unit by machining mirror-image upper and lower yoke halves, each with poles for several magnets. For example, a sector unit may consist of a dipole flanked by a pair of sextupoles and quadrupoles. Channels are cut around each pole for coils, leads and cooling lines. The yoke halves are also machined to accept a sector vacuum chamber. The two halves are then bolted together to form a self-supporting unit. One important advantage of this approach is that the magnets in the assembly are aligned relative to each other with CNC precision. Such an approach was used in the MAX-III ring in Lund, Sweden.

For fixed energy operation, permanent magnet (PM) driven dipoles offer an attractive energy-saving option. Trim coils would be incorporated for fine-tuning the field and even for varying machine energy over a limited range. Magnetic modeling of a gradient dipole using NdFeB has shown this approach to be feasible. A large volume of PM material would be required, so the initial cost is higher than for a conventional electromagnet. Assembly of magnets with large PM blocks is also more difficult because of the large magnetic forces that must be dealt with. However, life-cycle cost, factoring in the rising cost of electricity on Long Island, may make this option worth serious consideration.

3.4.3 Stored Current

The design goal for NSLS-II is a stored current of 500 mA to provide very high flux. There are several issues that arise as the stored current is increased. First, the heatload on vacuum chambers, absorbers, and beamlines increases. The heatload on accelerator components is considered in Section 3.4.8 and on beamline optics in Section 4.1. A second set of effects that become significant with increased stored current are various collective effects such as coupled and single bunch instabilities. These can lead to longitudinal oscillations (resulting in increased energy spread) and transverse oscillations (giving an increased effective emittance). Coupled bunch instabilities are discussed in detail in Section 3.4.5.1. We anticipate taking several steps to combat coupled bunch instabilities, including employing superconducting RF cavities, adding a harmonic cavity, and employing sophisticated feedback systems. RF systems are discussed Section 3.4.9 and feedback systems are discussed in Section 3.4.11.

At this point, we are confident we can achieve 500 mA. Further investigation during the conceptual design phase will be pursued to determine whether we can exceed this value.

3.4.4 X-ray Pulse Length

The natural electron, and therefore X-ray, pulse length for the current design of NSLS-II is expected to be only 11 psec (rms). This is shorter than any other storage ring and will be well suited to the range of timing experiments described in Section 2. However, as discussed below, these very short pulses combined with the high average current of NSLS-II result in very high peak currents per bunch. This has several negative consequences, including lower collective effect instability thresholds, shorter stored electron beam lifetimes, and increased heating of insertion devices.

Since the percentage of experiments that require such short pulses is expected to be relatively small, we currently envision running NSLS-II in two different operating modes. In fast timing mode, NSLS-II would be operated with the short pulses. However, in the normal operations mode that is expected to be the dominant operating mode, a passively powered third harmonic RF system (described in Section 3.4.9.1) would be used to stretch the electron bunch length. With this system, we expect the bunch length to roughly triple, resulting in an electron bunch length (and X-ray pulse time) of 33 psec (rms), which, while still quite short, greatly alleviates the effects mentioned above.

3.4.5 Collective Effects

NSLS-II will operate with electron bunches having both very low emittance and large charge per bunch. The bunches interact with themselves and with each other, coupled by the impedance of the vacuum chamber and other storage ring components, higher order modes (HOMs) of the RF cavities, coulomb scattering, and residual gas ions. This gives rise to various collective effects that can limit the stored current due to instabilities, reduce the lifetime of the stored current, and lead to energy spread or emittance blowup. The NSLS-II design parameters are aggressive and the design is especially challenging in this regard. In addition, NSLS-II will employ a large number of small gap undulators that significantly contribute to, and for the vertical plane even dominate, the impedance seen by the electron beam. Finally, since the electron energy of NSLS-II is intermediate at 3 GeV, it provides high brightness hard X-rays by utilizing the higher harmonics of the undulator radiation. This limits the allowable energy spread growth of the electron beam.

The collective effects are driven by interaction of the bunch with the electromagnetic field supported by the ring components, which is modeled as an impedance seen by the beam. As we develop the full conceptual and engineering design of the storage ring and its components, the full impedance will be calculated and the collective effects will be analyzed in detail. This process is typically iterative, whereby some of the components will be modified to reduce their contribution to the impedance and therefore raise the thresholds for various instabilities.

Here we present conclusions from our preliminary analysis of the collective effects based on estimates of the largest contributions to the impedance and the worst case situation corresponding to the higher peak currents encountered in fast timing mode.

3.4.5.1 Coupled Bunch Instabilities

Coupled bunch instabilities can be driven by the resistive wall impedance of MGUs and the rest of the vacuum chamber. The corresponding instability thresholds have been calculated analytically using some simplifying assumptions, such as infinite thickness of the vacuum chamber wall. If the MGUs are operated at room temperature, the shortest growth time of the longitudinal coupled-bunch modes is ~ 50 seconds and even longer if the MGUs are operated at 4.2 K. This is far greater than the damping time and therefore unimportant.

In the transverse case, the situation is quite different. This is primarily due to the MGU transverse impedance, which scales as $1/a^3$, where 2a is the MGU gap and can be as small as 5 mm. If the MGUs are operated at room temperature or 4.2 K, the instability growth time is found to be 0.25 ms or 2.9 ms, respectively. Both of these are shorter than the damping time, indicating that the transverse resistive wall instability may have to be stabilized by dedicated transverse feedback dampers.

Coupled bunch instabilities can also be driven by HOMs of the RF cavities. The instability thresholds due to longitudinal and transverse HOMs of several RF cavity designs have been estimated with simplified expressions and compared with growth rates calculated by ZAP. The PEP-II normal conducting cavities, and the KEK-B, CESR and SOLEIL superconducting cavities have been analyzed for longitudinal stability and the KEK-B superconducting cavity has been analyzed for transverse stability.

The results show that all of the cavities result in longitudinal coupled bunch instability threshold currents above the NSLS-II design values. The worst case is for the PEP-II cavity, where the HOM impedance is quite close to the threshold and some care is needed to ensure that the modes are stagger-tuned among the up to three cavities NSLS-II, which is easily satisfied. We conclude that any of the cavities appear to satisfy the requirements, although the superconducting cavities have a factor of 5-10 margin over normal conducting cavities.

Similarly, for the transverse coupled bunch instability the growth time of ~34 ms is about three times higher than the transverse damping time and so the KEK-B superconducting cavity does not cause transverse coupled bunch instability for up to 2 cavities in the ring. In the case that three cavities are required, the modes are of such low Q that it is no longer possible to stagger tune the HOM's and a feedback system may have to be added to damp this instability. In principle this could be the same system as the one that damps the resistive wall driven instability described above.

In summary, by utilizing feedback damping systems and superconducting RF cavities, coupled bunch instabilities are not expected to present any difficulties for NSLS-II operating in fast timing mode. When operated in normal mode with the harmonic cavities, the reduced peak current (as well as Landau damping from the harmonic cavities) is likely to make the feedback damping system unnecessary.

3.4.5.2. Single Bunch Instabilities

Single bunch instabilities can be driven by the broad band impedance of the vacuum chamber. Typically, this comes from many elements, including Beam Position Monitors (BPMs), scrapers, vacuum slots, various transitions, etc. Analyses to date have been based on scaling this impedance from other rings using simplified models. For example, measurement data from the current NSLS VUV/IR ring is well described by a Q = 1 broad-band resonator model with resonance frequency f_{BB} = 1.8 GHz, and $R_{shunt}/n \sim 1$ Ohm, where R_{shunt} is the shunt impedance. Scaling this with the effective vacuum chamber radius gives, for the NSLS-II ring, f_{BB} = 2.9 GHz, and $R_{shunt}/n \sim 1.6$ Ohms.

In the case of NSLS-II with many MGUs, small gap transitions are expected to dominate the transverse impedance in the vertical plane. It has also been confirmed by recent NSLS measurements that the geometric contribution greatly exceeds the contribution from the resistive wall. In the limit of low frequencies, the transverse impedance of a linear taper is essentially inductive and scales quadratically with the tapering angle. To be in this regime, however, the taper should be long, $L_{taper} >> h\ a\ /\ \sigma_z$, where h is the nominal vacuum chamber height, σ_z is the bunch length, and a small transverse aspect ratio is assumed for simplicity. Estimates for the parameters of NSLS-II result in a minimum taper length of about 15 cm, however longer tapers should be planned to lower the magnitude of the impedance. Design of a tapered variable gap chamber will be more complex. To develop these designs, we intend to embark on an R&D program that includes wake-field calculations with 3D EM field solvers, bench measurements of impedance for a prototype chamber, as well as detailed analysis of single bunch transverse instability thresholds.

We have also made preliminary estimates of the longitudinal instability threshold. Estimates in the mode coupling regime, $\lambda_{wake}/\sigma_z >> 1$, indicate that the above estimated impedance gives a current

instability threshold that is rather close to the NSLS-II single bunch current. Note, however, that the NSLS VUV/IR vacuum chambers were constructed without detailed impedance considerations, and it is expected that the NSLS-II impedance values will be lower by an order of magnitude or more.

In the microwave instability regime, $\lambda_{wake}/\sigma_z << 1$, the well-known Boussard criterion for the onset of the microwave (MW) instability indicates that the broad-band impedance, $|Z_n/n|$, must be less than ~ 0.1 Ohms. It is widely believed that such impedance values are achievable. For example, detailed calculations of the damping ring impedance of the Next Linear Collider produce $|Z_n/n|$ numbers an order of magnitude lower [1]. Also, it is important to note that the longitudinal impedance is not expected to be affected much by the MGUs. Furthermore, if the impedance is purely inductive rather than resistive, the beam is stable for all currents. In principle, CSR impedance might also contribute to the MW instability. However, our preliminary estimates for the CSR induced instability at NSLS-II indicate a relatively high threshold, so this is not a problem.

In summary, by careful control of the taper of the MGU transitions and the broadband impedance of the NSLS-II storage ring components, single bunch instabilities should not present any difficulties for NSLS-II operating in either fast timing mode or in normal mode.

3.4.5.3 Intra-Beam Scattering

While strictly speaking not a collective effect, intra-beam scattering (IBS) is often considered together with collective effects. IBS may degrade beam quality since it generally results in six-dimensional phase-space growth of the beam. The magnitude of the effect is proportional to the particle phase-space density and scales inversely with the square of beam energy. We have done SAD simulations that indicate that the maximum relative blow-up is only a few percent at 1.5 mA single bunch current, which is about twice the nominal single bunch current for standard multi-bunch operation. This and other considerations give us reasonable confidence that IBS should not be a factor for NSLS-II operating in fast timing mode and even less so for normal mode operations. However, IBS may become important for some very specialized modes of operation, such as very high single bunch charge.

3.4.5.4 Ion-related Instabilities

Finally, we note that there also exists yet another class of instabilities due to the interaction of beam electrons with ions and low energy electrons in the vacuum chamber, which are produced by various mechanisms. Although these instabilities have not been considered to date, they will be analyzed in detail during conceptual design. This is especially important for MGU locations, where the small transverse beam size may drive ion-related instabilities and providing adequate pumping in a long small gap presents a challenge.

3.4.6 Effects of Insertion Devices

The impact of individual undulators on the electron beam properties can usually be ignored. However with as many as 20 small gap undulators installed in the ring the impact on the electron beam needs to be considered. We have estimated the impact assuming the worst case of maximum K, and hence maximum magnetic field, B. The undulators considered are the superconducting undulators U14 (λ = 14 mm, K_{max} = 2.24, length = 5 m) described in section 3.4.12. We find that the energy losses will be easily handled by the RF system since even with 20 U14 undulators operating at K_{max}, the loss is only 66 % of the dipole loss.

A second potential impact is a change in the electron emittance. This is always to lower values and is related to the ratio of $[\rho_{dipole}/\rho_{undulator}]$ as well as the integral of the dispersion emittance over the undulator. For the U14, this ratio is ~ 1.25. While the emittance reduction is small per undulator (~ 1 to 2 %), 20 undulators could result in a significant reduction of ~ 40%. This has the potential to drive the emittance

below 1 nm for even higher brightness. The energy spread is also related to this ratio and therefore a small increase may occur for 20 U14 undulators all operating at K_{max}, but this is not expected to be significant.

Finally, the tune shifts are quite small and shouldn't be a problem even with 20 U14 undulators. However, if they are all operating at K_{max} some tune correction may be required with the quadrupoles.

3.4.7 Electron Beam Lifetime

Electron losses due to finite energy acceptance or limited transverse dynamic or physical apertures contribute to limit the lifetime of the stored electron beam. We consider these in turn to arrive at the expected overall lifetime for NSLS-II.

3.4.7.1 Quantum Lifetime

Photon emission by synchrotron radiation generates electron energy spread, with rms value σ_ε. This results in the so-called quantum lifetime, τ_q, which is given by

$$\tau_q = \frac{\tau_\varepsilon}{2}\frac{e^\xi}{\xi},$$

where τ_ε is the energy damping time and $\xi \equiv \varepsilon_{RF}^2 / 2\sigma_\varepsilon^2$ is the scaled RF energy acceptance, ε_{RF}. Similar expressions, with corresponding damping times and limiting half apertures, hold for the transverse dimensions. Unless the apertures are extremely small (<10 times the beam size) the quantum lifetime is essentially infinite. Since for NSLS-II, both the RF acceptance and the transverse limiting apertures will significantly exceed the beam dimensions the quantum lifetime can be ignored.

3.4.7.2 Gas-Scattering Lifetimes

The gas scattering lifetime due to elastic collisions between the stored electrons and gas nuclei is given by

$$\frac{1}{\tau_{scat}} = \frac{4r_e^2 Z^2 \pi n c}{2\gamma^2}\left[\frac{\langle\beta_x\rangle\beta_{x,max}}{a^2} + \frac{\langle\beta_y\rangle\beta_{y,max}}{b^2}\right]$$

where n and Z are the nuclei concentration and charge respectively, and a and b are the horizontal and vertical stay clear apertures. In case of NSLS-II, the vertical acceptance (defined as the minimum value of b^2/β_y over the circumference) is limited by the MGUs. Since it is expected to be significantly smaller than the horizontal acceptance we will consider the vertical contribution to the lifetime only. For the TBA lattice and 2 m long, 5 mm full gap NSLS-II MGUs, the vertical acceptance is 2.24 μm-rad. Calculating n from the usual conservative assumption of 1 nTorr N_2-equivalent pressure gives the elastic gas-scattering lifetime of $\tau_{scat} \approx 61$ hours.

It should be noted that the largest acceptance is reached when the beta function in the center of the straight, β*, equals half the length of the insertion device (ID). Therefore, for given ID length, the gas scattering lifetime could be lowered further by reducing the vertical beta function. Alternatively, for the present lattice with β* = 2.37 m IDs of up to ~5 m in length (again assuming 5 mm full gap) could be used without compromising gas-scattering lifetime.

Bremsstrahlung on nuclei of residual gas, or inelastic gas scattering, may lead to particle loss when the momentum of the scattered electron is outside the limiting momentum aperture ε_{max}. The corresponding lifetime can be written as

$$\frac{1}{\tau_{brem}} = \frac{16 r_e^2 Z^2 nc}{411} \ln\left[\frac{183}{Z^{1/3}}\right]\left[-\ln\varepsilon_{max} - \frac{5}{8}\right].$$

In principle, either physical aperture, dynamical aperture, or the RF bucket height may set the momentum aperture. The bremsstrahlung lifetime, when calculated for 1 nTorr N_2-equivalent pressure and a 3% limiting momentum aperture, is $\tau_{brem} \approx 72$ hours.

As discussed in Section 3.4.12.4, the present superconducting MGU concept assumes cold-bore devices operating at liquid He temperatures with cold surfaces directly facing ring vacuum. Inside the superconducting MGU chamber the above assumption of 1 nTorr N_2-equivalent pressure is irrelevant, since most gas species (including N_2) will likely cryopump to much lower pressures. This however, does not apply to He itself, which in principle may contaminate the ring vacuum inside the superconducting MGU chamber. He is hard to remove and even with state-of-the art vacuum technology one should expect the residual pressure to remain in the 10^{-8}-10^{-7} Torr range. Assuming the most pessimistic pressure of 10^{-7} Torr He-equivalent, the gas scattering lifetime estimates given above would be lower by a factor of ~4. However, this reduction hardly changes the overall gas scattering lifetime, since the superconducting MGUs occupy only a small fraction of the ring circumference. Therefore, for practical purposes, the effect of the superconducting MGUs on the gas scattering lifetimes can be ignored and the estimates above based on 1 nTorr N_2-equivalent pressure estimates can be used.

3.4.7.3 Touschek Lifetime

Coulomb scattering of charged particles in a stored beam causes an exchange of energy between the transverse and longitudinal oscillations. The Touschek effect is the transformation of a small transverse momentum into a large longitudinal momentum due to scattering and can lead to loss of particles that fall outside the momentum limiting aperture. Unlike gas scattering, the time dependence of the number of stored particles is not exponential but is rather described by

$$N_b(t) = \frac{N_b(0)}{1 + t/\tau_{tous\_1/2}}$$

Here, $\tau_{tous\_1/2}$ is the so-called Touschek half-life. For short time intervals, such as the ones that occur between top-off injection pulses, the inverse half-life directly gives the slope of $N_b(t)$. Alternatively, for longer time periods, when $N_b(t)$ can no longer be considered linear, its time dependence can be approximated by an exponential with lifetime $\tau_{tous} = \tau_{tous\_1/2}/\ln(2) \approx \tau_{tous\_1/2}/0.693$. This regime is less relevant for NSLS-II, and therefore we will use $\tau_{tous\_1/2}$ to estimate particle losses.

The Touschek lifetime for NSLS-II was calculated with three different codes, SAD, ZAP, and MAD, which showed good agreement. So far, no physical or dynamic apertures have been explicitly put in. The lifetime versus RF bucket height for 500 mA current and 3 GeV ring energy is shown in Figure 3.4.3 (top). The Touschek half-life also has a strong dependence on ring energy, as shown in Figure 3.4.3 (bottom) assuming 3% RF bucket height and 500 mA total current. At 3 GeV, $\tau_{tous\_1/2}$ = 2.4 hours; it quickly grows at higher energies.

The Touschek lifetimes estimated above are for NSLS-II operating in fast timing mode (see Section 3.4.4). Since the Touschek lifetime is proportional to the bunch length, it is expected to triple to around 7.2 hours in the normal operating mode.

Finally, we note that these lifetime estimates are preliminary as several mechanisms may substantially modify the Touschek numbers above. These will be studied further during the full conceptual design for NSLS-II. Specifically, the momentum acceptance may be limited due to dynamic aperture (which is momentum dependent and has to be calculated for large momentum deviations), non-linear momentum compaction, synchrotron oscillations (which reduce the dynamic aperture due to higher order chromaticity), magnet alignment errors (which affect the emittance coupling), and small gaps of the MGUs (due to coupling, Touschek scattered particles in the beam halo may get lost on vertical apertures). In the future, particle tracking with some or all of the above will be performed with the full lattice, magnet errors, and physical apertures.

3.4.7.4 Total Lifetime

While all the mechanisms considered so far contribute to the overall lifetime, the Touschek losses are clearly the dominate ones for NSLS-II. In fact, adding all the contributions considered so far, and assuming 3% limiting momentum acceptance, gives an overall lifetime when operating in fast timing mode of 2.2 hours or, using τ_{tous} rather than $\tau_{tous\_1/2}$, of 3.1 hours for longer time-scales. In the normal mode of operations, the overall lifetime will be 5.9 and 7.9 hours for short and long time-scales, respectively. Since the overall lifetime is very close to the Touschek-only number, longer IDs should be possible without significantly impacting the overall lifetime.

3.4.8 Heat Loads

To achieve its aggressive brightness and flux goals, NSLS-II will utilize high stored current and long small-gap undulators. This can result in a substantial heat load on accelerator components from a number of mechanisms, including both incoherent and coherent synchrotron radiation from the bending magnet dipoles and undulators, 'geometric wake heat', image current (also known as resistive wall, or Ohmic) heating, and others. These will be carefully taken into consideration during the engineering design stage once the ring components become better defined.

At the present time, we have considered only one component, specifically the superconducting undulator chamber, as this component is one of the most challenging in terms of handling the heat load. Present superconducting undulator design (see Section 3.4.12.4) includes a Cu-coated inner chamber cooled to liquid He temperature (4.2 K) with 2a = 5 mm full vertical gap. The amount of heat induced by the beam in this chamber affects the feasibility of the cryogenic design. Of the many mechanisms of beam energy transfer into the ID vacuum chamber, at this point image current heating is believed to be the most important.

We estimate the image current induced power per unit length, P/L, for undulators at room temperature. Using the normal skin effect surface impedance and Gaussian electron bunches of rms length σ_z we find $P/L \sim I^2/(\sigma_z^{3/2}\, a)$, where only the dependence on current, bunch length, and chamber aperture is expressed. A conservative estimate of the power deposited per unit length results in ~ 25 W/m in fast timing mode (short σ_z) and ~ 5 W/m in normal operating mode. Either of these values is insignificant for a superconducting undulator in a warmed-up state.

The situation is different when the superconducting undulator is cold and for the frequencies corresponding to the few mm bunch-length of interest. In that case, the Cu coating of the superconducting undulator chamber is expected to be in the extreme anomalous skin effect regime and we find $P/L \sim I^2/(\sigma_z^{5/3}\, a)$. When estimated for NSLS-II parameters we find P/L ~ 5 W/m in fast timing mode and ~ 0.8 W/m in normal operating mode. While these power levels are significantly down from the room temperature values, they now have to be removed cryogenically. Currently, commercial cryo-coolers are available with a capacity of up to 1.5 W. Thus it will likely be necessary to combine several cryo-coolers, provide dedicated refrigerators for each superconducting undulator, or perhaps have a central cryo-plant, with liquid He plumbed around the ring to all superconducting undulators.

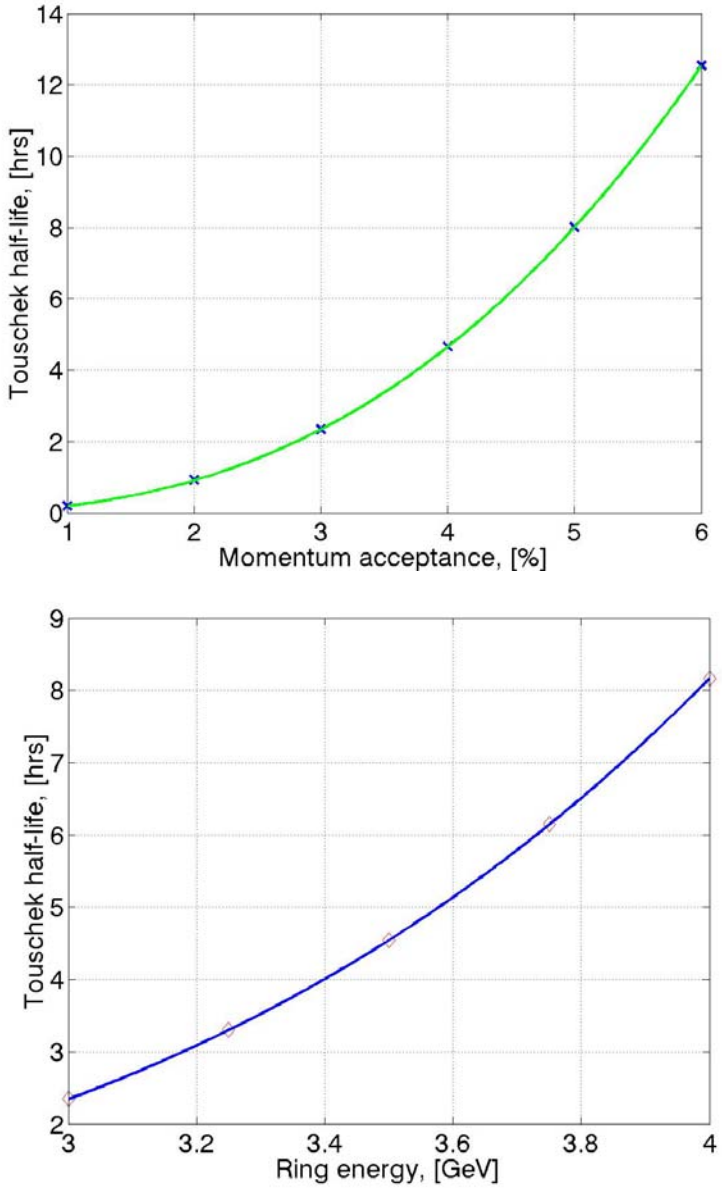

Figure 3.4.3 *Touschek half-life versus momentum acceptance (i.e., RF bucket height) (top) and versus X-ray ring energy (bottom).*

It is important to note that, while encouraging, these results are preliminary and are based on a simplified treatment that will be further refined during conceptual and engineering design.

3.4.9 RF

The NSLS-II RF system must provide sufficient voltage to deliver an acceptance greater than the beam size throughout the operating regime, and power to the beam to make up the synchrotron radiation losses. This amounts to 2.8 MV for a 3 % momentum acceptance in a 500 MHz RF system assuming 870 kW for radiation losses with the full complement of insertion devices.

Both normal conducting and superconducting cavity systems have been considered, with a superconducting system being the preferred choice at this point for several reasons: fewer cavities are

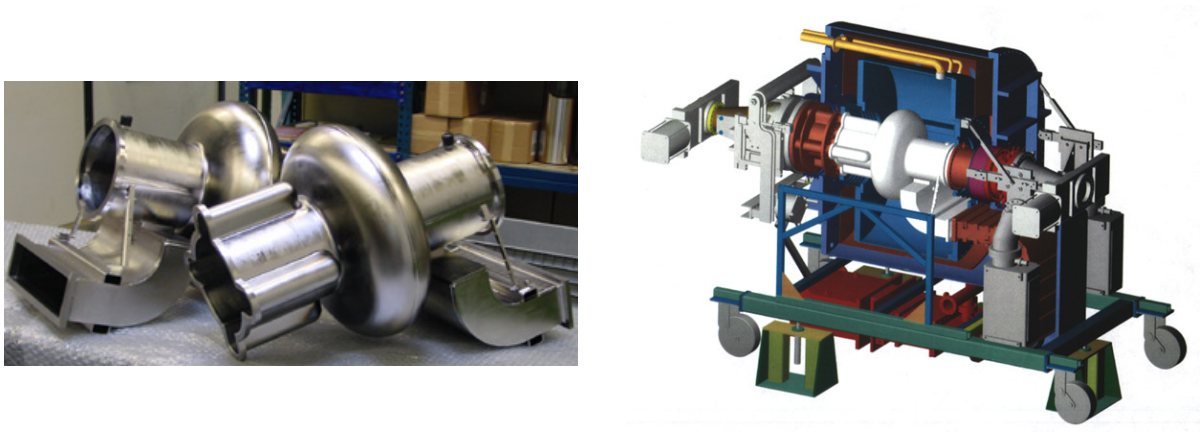

Figure 3.4.4 *Superconducting 500 MHz CESR RF cavity developed at Cornell.*

required resulting in fewer straight sections being used to house the cavities; lower installation and operating costs; and lower HOM impedances that result in a stable electron beam without the need for additional complexities in the feedback systems in order to tame HOM driven coupled bunch instabilities

Both the KEK-B and Cornell CESR-B superconducting RF cavity designs were analyzed for HOM impedance contributions to coupled bunch instabilities and found to be unconditionally stable (see Section 3.4.5.1). The CESR cavity is shown in Figure 3.4.4. Both have similar power coupling capability and both are available commercially. Either system will meet the requirements for NSLS-II. For purposes of illustration, a KEK derived system is outlined in the following paragraphs.

The KEK-B cavity easily meets the voltage requirement of 2.8 MV with a single cavity, however a minimum of two cavities are required to meet the 800 kW beam power. Existing fundamental power couplers have been operated at 380 kW each, and bench tested higher. Since the superconducting RF cavities with 500 mA of beam loading cannot be always operated as a matched load the couplers must exceed this power level. We are investigating adopting the KEK-B cavity design to add a second input coupler to each cavity. This would give us ample margin to fully power each cavity. Therefore, two cavities are anticipated at this time. The total length of two cavities is ~ 5.4 m, so they will fully occupy one of the 7 m straight sections.

Each cavity will have its own RF power source. CW klystrons with output power between 500 and 1000 kW are commercially available. Alternatively, Inductive Output Tubes (IOT's), which have higher efficiency although at lower gain, have been built at 700 MHz with an output power of 700 kW and can be easily scaled to operate at 500 MHz. These tubes have the important advantage of being able to provide very high instantaneous output power that, when coupled with their low group velocity, allows them to be designed into feedback loops around the cavity for control of the cavity fundamental impedance, greatly improving the beam-loading problem. A single IOT per cavity is thus anticipated.

3.4.9.1 Third Harmonic Superconducting RF Cavity for Bunch Lengthening:

The short bunches (11 psec, rms) produced by the low momentum compaction of the low emittance lattice result in a short Touschek lifetime (see Section 3.4.7.3) and increased image current heating of superconducting undulators (see Section 3.4.8). As explained in Section 3.4.4, we plan to operate in two modes: a fast timing mode with 11 psec (rms) pulses and the normal operating mode with 33 psec (rms) pulses. This longer pulse length will be obtained by installing a third harmonic RF cavity to stretch the electron bunch. A third-harmonic cavity of the type developed for BESSY II by Accel Instruments will be sufficient for this purpose.

3.4.10 Injection System

The low emittance of the high brightness lattice of NSLS-II results in quite a short lifetime. This makes operation in top-off injection mode a necessity. Some of the other benefits of top-off operation include constant heat load on accelerator components and beamline optics for increased stability, and constant intensity delivered to experiments.

We begin discussion of the injection system for NSLS-II by considering the requirements for top-off operation of NSLS-II. Our goal is to maintain the storage ring current constant to within 1%. The lifetimes in fast timing and normal operating modes were estimated in Section 3.4.7.4 to be 2.2 and 5.9 hours. As discussed there, these preliminary lifetime estimates may become even shorter as additional development is done during the conceptual design. From the parameters listed in Table 3.4.1, we thus need to replenish about 1% of the charge, or about 0.015 nC, in each filled bunch about once per minute. If we inject at 10 Hz, we could top-off each bunch with this charge once per minute and maintain the bunch charge constant to within 1%. Alternatively, if we accept bunch-to-bunch charge variations of 10% while still maintaining the average current constant to 1 %, we could inject 0.15 nC at a 1 Hz rate. We note that even at the faster 10 Hz injection rate, the 100 ms between injections is still more than 10x greater than the damping time required for the injected charge to reach equilibrium.

In addition, the expected small dynamic aperture and low emittance of the NSLS-II storage ring also implies that the emittance of the injected beam must not be much larger than that of the stored beam to achieve acceptable injection efficiency. Based on experience at the Swiss Light Source and elsewhere, we plan for the emittance of the injected electrons to be no more than a factor of ten larger than the equilibrium emittance in the main ring, i.e., it should be less than 15 nm.

These injection charges, rates, and emittances can be achieved with either a low energy linac driving a full energy booster synchrotron or a full energy linac, and we consider both below. We conclude that there may be advantages to utilizing a full energy linac injection system and this is included in our current plans.

3.4.10.1 Booster Synchrotron

If we use a booster synchrotron injection system, we envision an 800 MeV linac feeding a full energy booster for acceleration of electrons to the 3 GeV energy of the X-ray ring. The linac provides full energy injection of the IR ring as well as serving as an injector for the booster. The booster design has to provide rapid filling of the X-ray ring, flexible repetition rate and ramping profile, and meet the injection charge, efficiency, rep rate, and emittance requirements outlined above. Our preliminary design of a booster injection system that meets these requirements includes a thermionic gun, prebuncher and buncher cavities, linac, linac to booster transfer line, and booster lattice.

A gridded cathode thermionic gun can provide 1 nsec, 1.5 nC electron pulses for single bunch operation. Provision for 500 MHz modulation of long (~100 ns) macropulses for bunch-train injection to the ring will also be explored. A gridded thermionic gun has the advantage of easily varying the charge per bunch between 0.1 and 1.5 nC by varying the bias voltage, allowing the top-off charge per bunch to be continuously adjusted to achieve steady state currents.

Since the thermionic gun cannot make pulses less than 1 ns, and a linac RF bucket is a maximum of 0.33 nsec long a minimum of 3 linac bunches are created. A 500 MHz prebuncher is used to modulate the energy of the electron pulse such that a subsequent drift will create a high-density central bunch at the expense of the two outside bunches. In long-pulse operation the prebuncher acts to sweep particles away from the ends of the separatrix where there is zero bucket height, towards the center where phase errors will result in smaller energy oscillations as the off-center linac bunches undergo coherent synchrotron oscillations.

A 2.997 GHz RF buncher is used to improve the capture efficiency of the linac by moving particles away from the edges of the separatrix. This will be a few cells of 2.997 GHz structure fed either from a

small independent amplifier, or with a few kW siphoned off parasitically from the first klystron waveguide feed to a linac tank with high-power phase and amplitude control.

A linac frequency of 2.997 GHz is chosen, which is a 6th harmonic of the RF ring frequency of 499.654 MHz. It is constructed of iris-coupled traveling wave structures similar to the SLAC MK IV linac. Each tank will be driven by a 45 MW peak power klystron. Full turn injection into the booster requires a macropulse length of 500 ns, which is easy to accommodate into the flat top of the klystron Pulse Forming Network. Actual pulse length will be less due to injection and extraction kicker rise and fall times.

The requirements for the linac to booster and linac to IR ring transfer lines are very similar to those for the one at the existing NSLS. An energy analyzing slit will be placed in the bend to limit the energy. A thermionic gun cannot produce pulse lengths shorter than ~1ns, and so the booster RF bucket must accept a linac bunch train of 3 successive bunches, which are within the longitudinal acceptance of the 500 MHz booster bucket.

To achieve the desired low emittance in a compact space the booster design is based on a simple "gradient FODO cell" that makes use of a combined function dipole to provide bending and to also serve as an effective defocusing quadrupole for the cell. Dispersion suppressors are added to the arcs to produce dispersion free straight sections for injection, extraction and the RF system. Even with this compact design, the booster has a substantial circumference of 165 m.

A schematic layout of this design is shown in Figure 3.4.5. While this design meets most of the requirements, its rep rate will only be 3 Hz, which is marginal. Even at this rate, the booster is essentially

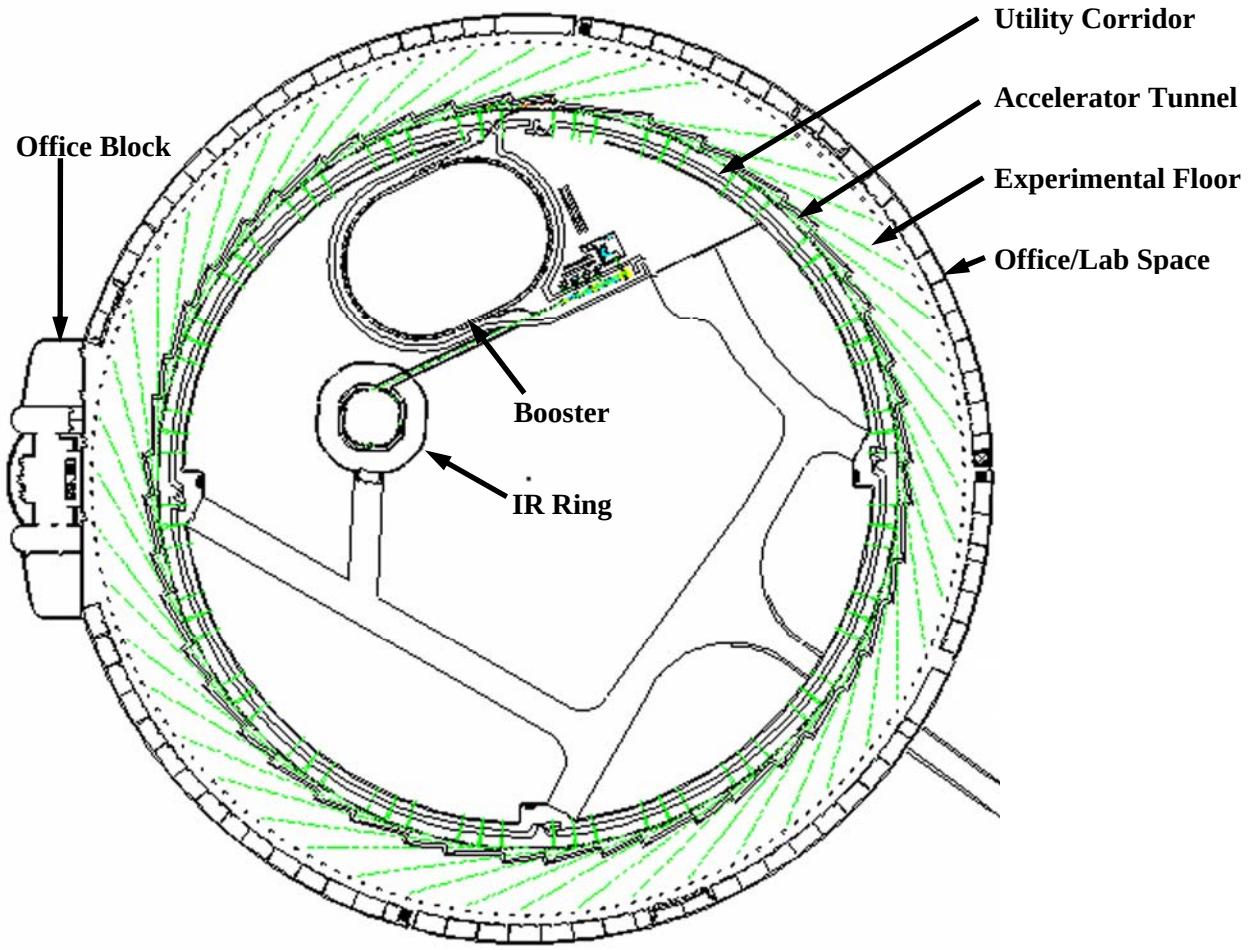

Figure 3.4.5 *Schematic of NSLS-II with a full energy booster synchrotron and linac pre-injector. The linac pre-injector also serves as a full energy injector for the IR ring.*

continuously ramping, which creates increased operating cost and reliability concerns. The possibility of using multi-bunch injection to lower the injection frequency will be explored during development of the full conceptual design.

3.4.10.2 Full Energy Linac Injector

An attractive alternative to a booster synchrotron is a full energy linear accelerator. As shown in Table 3.2.1, two existing light sources use full energy linacs as injectors, and one of these (Pohang Light Source, PLS) uses it in the more demanding top-off mode. A full energy linac is also used as a full energy injector for three storage rings dedicated to high energy physics (KEK ATF, KEK B-Factory, PEP-II B Factory) and all of these also operate in top-off mode.

A full energy linac injector for NSLS-II has the following potential advantages:

- ***Higher Rep Rate***: A linac can be operated from a few Hz up to 120 Hz with more or less the same hardware, while a booster becomes increasing difficult for rep rates beyond a few Hz due to eddy currents in the vacuum chamber and the complexity and cost of fast ramping power supplies.

- ***Better Beam Quality***: If the linac is coupled to a laser driven photoinjector that produces a 1.5 nC/bunch electron beam with a normalized emittance of 6 μm, the geometric emittance of this electron beam at 3 GeV would be ~1 nm, which is smaller than the horizontal emittance of the storage ring (~1.5 nm) and an order of magnitude smaller than the emittance from the booster presently under consideration.

- ***Better Injection Efficiency***: The better beam quality discussed above will result in better injection efficiency. The KEK ATF recently demonstrated nearly 100% injection efficiency with a photoinjector/linac system. Better injection efficiency is especially important for a high current storage ring operating in top-off mode. It can provide a significantly lower radiation background during 'shutters open' top-off injection, resulting in minimized radiation damage to undulators and reduced shielding (and hence reduced cost) requirements.

- ***Flexibility in Ring Filling Patterns***: Both single pulse and pulse train injection has been experimentally demonstrated with full energy linac injectors. Furthermore, variable fill patterns and charge/bunch can be easily implemented for the linac with a photoinjector.

Historically, a low energy linac with a full energy booster has been the choice for most light source injection systems because of its perceived advantages in cost and reliability. However, as pointed out above, these are much less compelling at the injection rates required for NSLS-II. In addition, developments in normal conducting linac technology, such as SLED, high power klystrons, and solid state modulators, make a full energy linac injector a very attractive alternative. Recent developments in photocathode RF gun technologies, especially in stability and reliability, make it compatible with storage ring operation. Diode-pumped, all solid state lasers and semiconductor, saturable absorber based passive mode locked oscillators have improved the laser system stability and reliability tremendously. Both metal cathodes (Mg) and semiconductor cathodes (Cs_2Te) have demonstrated lifetimes of more than several months with a quantum efficiency better than 0.1%. A photocathode RF gun injector is now in routine operation for the damping ring at KEK ATF.

In view of these considerations, we see this as an attractive choice. However, we will continue to evaluate the relative merits of both booster and full energy linac injection systems as part of the conceptual design phase of the NSLS-II project.

3.4.11 Photon Beam Stability

To realize the benefits of the high brightness and small beam sizes of NSLS-II, it is essential that the photon beams be exceedingly stable. The stability requirements include constant intensity after apertures, constant photon energy after monochromators, and minimal photon source size and highly precise steering accuracy for focusing on small samples. These requirements directly translate to electron beam current and orbit stability (considered here) combined with stability of beamline components (considered in Section 4.1).

Disturbances with frequencies higher than the experimental sampling rate are generally less harmful since they usually average out and only linearly increase the effective emittance $\varepsilon_{eff} = \varepsilon_0 + \varepsilon_{cm}$, where ε_0 is the emittance without noise and ε_{cm} is the emittance defined by the ellipse of the centroid motion. For example, 5 % fluctuations in centroid motion and divergence results in a 0.25 % increase in effective emittance. However, when disturbances are on a frequency comparable to the sampling rate, their contribution to the effective emittance is more pronounced, $\varepsilon_{eff} \sim \varepsilon_o + 2\,(\varepsilon_o \times \varepsilon_{cm})^{1/2} + \varepsilon_{cm}$, so that the same 5% motion result in a 10% increase in emittance. Finally, while beam motion on timescales longer than the duration of an experiment have little effect on it, reduction of such motions is still desirable in order to eliminate or reduce realignments.

From these considerations we arrive at our stability requirements of no more than 10% beam motion, both positional as well as angular, particularly in the frequency range from ~ 10 mHz to 1kHz. For the current NSLS-II design parameters, this implies that the rms beam position is stable to within 5 (0.4) μm and the rms beam angular direction is stable to within 3 (0.4) μrad, in the horizontal (vertical) directions, respectively.

Achieving the requirements for NSLS-II will require advancing the state of the art, with improved construction and feedback stabilization techniques. However, NSLS is well qualified to accomplish this. NSLS has a rich history of accomplishments in the area of orbit stability, including the invention of switched beam position monitor (BPM) receivers, global orbit feedback, novel compensation techniques for fast switching IDs, and pioneering developments in digital orbit feedback, among others. The digital orbit feedback systems we have recently implemented have the world-highest update rate and correction bandwidth, and maintain the vertical beam position stabile to within a few microns in a 0.25-150 Hz bandwidth.

Common sources of orbit motion that must be overcome include: ground motion; floor vibrations due to in-house machinery; thermally induced motion of ring components; injector induced electrical noise; magnet power supply noise; and the effects of a large number of independently controlled IDs (including some that are fast switching). Fortunately, due to extremely well settled glacial sands, ground stability at the proposed NSLS-II site is extremely good, and is definitely superior to that at many existing light sources. This applies both to the natural settlement/noise as well its ability to damp noise sources such as vehicular traffic.

Top-off operation of NSLS-II will be essential in providing good beam stability on slower timescales. Some of the major benefits of topoff injection for stability include: constant heat load on beamline optics and ring components; elimination of magnet ramping and associated effects (heat transients, hysteresis, eddy current induced stresses and mechanical motion, etc); and relaxed requirements for BPM accuracy versus beam current.

One drawback that accompanies topoff injection is a constantly running injection bump that can never be perfectly closed. For example, at the Swiss Light Source, the residual vertical orbit distortion in the undulators is ~ 30 μm. This motion is present only with the bump on and dies away on the timescale of a damping time when the bump is off, so its contribution to the orbit stability to a large extent averages out. Nevertheless, NSLS-II will likely have to employ sophisticated active compensation systems to reduce or minimize the residual beam motion elsewhere in the ring.

At this point, the most significant orbit stability issue for the NSLS-II appears to be the ability to measure extremely small orbit motions. This will require novel BPMs with full bandwidth resolution of

0.1 μm or better, as well as mechanical innovations for BPM mounting (starting from the girders and up). Reducing thermal expansion of ring components such as BPM mounting stands to acceptable levels will require maintaining the temperature in the storage ring tunnel to 0.1^{o} C or better. Minimizing vibrations will require techniques such as designing mechanical components to avoid low frequency resonance modes, using viscoelastic dampers, and using girders to support entire sections of the ring components.

Advanced orbit position measurement techniques and advanced mechanical construction techniques will enable sophisticated feedback/feedforward systems. In addition to electron beam parameters and accelerator settings, these systems will monitor and control mechanical motions of various accelerator and beamline components. Together, these approaches will achieve the required beam position and angular stability at NSLS-II.

3.4.12 Insertion Devices

3.4.12.1 High-Energy Undulator Sources

The most challenging requirements for high energy undulators come from programs that require high brightness, narrow-band, tunable, multi-kilovolt X-rays. Ideally, these photon energy ranges should be obtainable from undulators using the fundamental mode and the first few (odd) harmonics in overlapping bands, with no gaps in the coverage. However, with existing or anticipated magnet technologies, the requirement of fundamental resonance at 5 keV with wide tunability can be met only for electron beam energies of 6 GeV or higher (as at APS, ESRF and Spring8). In a medium-energy storage ring, tunable radiation at energies above 5 keV can be obtained from an undulator with a lower fundamental resonance energy, using its higher harmonics.

Insight into these constraints can be elicited from a few basic relationships governing planar undulators. The resonant fundamental wavelength, λ_1, of a planar undulator is given by

$$\lambda_1 = (\lambda_u / 2\gamma^2)(1 + K^2/2)$$

where λ_u is the undulator period, γ is the relativistic factor, B_o is the peak magnetic field, and the K factor is given by

$$K = 0.934\ \lambda_u\ [\text{cm}]\ B_o\ [\text{Tesla}]$$

The resonance condition can alternatively be expressed in terms of the fundamental photon energy:

$$E_1\ [\text{keV}] = 1.24 / \lambda_1\ [\text{nm}] = 2.48\text{x}10^{-7}\ \gamma^2 / [\lambda_u\ [\text{cm}]\ (1 + K^2/2)]$$

For 3 GeV electrons (γ = 5871) and K of order 1, to obtain E_1 = 5 keV would require an undulator period, λ_u, on the order of 1 cm. In fact, the first in-vacuum undulator (IVUN) installed at NSLS did have a period of 1.1 cm. However, a second key requirement for undulators is tunability, embodied in the factor $(1 + K^2/2)$, which varies with the magnetic field. For full spectral coverage between the fundamental and third harmonic this factor must vary by 3:1 for $K_{min} \leq K \leq K_{max}$. Since useful radiated power is only obtained for $K_{min} \geq 0.5$, a 3:1 tuning range requires $K_{max} \geq 2.2$. Thus, if we want the lowest energy of the tuning curve of the undulator fundamental to be 5 keV when K = 2.2, then we need a period of 0.5 cm. With this period, we then need a peak field of B_o = 1.66 Tesla in order to reach K = 2.2. To achieve such a high field with any currently available technology would require an unrealistically small magnetic gap on the order of 1 mm! At NSLS, both IVUN and its successor, the Mini-Gap Undulator (MGU), operate at an unprecedented minimum gap of 3.3 mm, which is permitted by an unusually small beta function (0.3 m).

Current lattice designs for NSLS-II call for a larger beta function (2.4 m) in the center of the straight. For undulators of length 5 m, a safe vertical stay-clear aperture of 5 mm has been specified. No existing technology can produce a (DC) magnetic field of 1.66 Tesla in a planar periodic structure with 0.5 cm period and 0.5 cm gap. However, if we allow a longer period of 1.4 cm or more, we can obtain both higher fields and adequate tunability, but with a lower fundamental energy. The 5-20 keV range may then be covered by the third and higher harmonics. We next describe two candidate undulator designs, one based on proven in-vacuum permanent magnet technology and the other on still-developing superconducting technology.

3.4.12.2 In-Vacuum Permanent Magnet Undulators

NSLS pioneered in-vacuum permanent magnet (PM) undulator technology nearly a decade ago. By placing the magnet arrays inside the vacuum envelope, the conventional vacuum chamber can be removed and the magnet gap can be reduced to the minimum stay-clear aperture. Since the peak undulator field increases exponentially as the ratio of the gap to period, g/λ_u, decreases, the period can also be reduced, raising the fundamental energy. Short-period, small-gap, in-vacuum PM undulators have thus brought kilovolt-level photon sources to medium-energy storage rings. Both pure-PM and PM-hybrid in-vacuum undulator designs are in service in many storage rings around the world. PM-hybrid (employing high-permeability poles driven by PM's) in-vacuum designs offer higher fields than pure-PM, and they have been proven in NSLS Mini-Gap Undulators (MGUs) and elsewhere.

For 5-20 keV coverage, we can allow the third harmonic to start at 5 keV. The lower fundamental energy, E_1, is then 1.67 keV. We may further relax the tunability requirement by allowing a gap between the first and third harmonics and only requiring continuous coverage between higher harmonics starting with the third harmonic. This reduces the necessary tuning range to 1.67:1, which can be obtained with K varying between 0.5 and 1.32. This constraint leads to $\lambda_u \leq 2.7$ cm.

A second constraint comes from achievable field with a given g/λ_u ratio. An updated version [2] of the Halbach design formula for peak field in a PM-hybrid undulator using modern NdFeB permanent magnets is

$$B_o = 3.694 \exp [-5.068 (g/\lambda_u) + 1.52 (g/\lambda_u)^2]$$

From this, we obtain a realizable PM-hybrid undulator design, designated MGU-19, with 19 mm period, 5 m length, and peak field of 1.06 T, giving a K_{max} of 2.24. The fundamental covers 1.63 to 4.0 keV, a tuning range of 2.44:1. However, continuous tuning is obtained from 4.9 to over 20 keV, using the third through eleventh harmonics. This model has been verified with the 3D magnetostatics code Radia.

In-vacuum MGUs can be tailored to other energy ranges as well. Another example, designated MGU-21, has a 21 mm period, 5 m length, peak field of 1.14 T and K_{max} of 2.24. This gives a tuning range of 3.13:1 and does provide full coverage from 1.15 to over 10 keV using the fundamental through the seventh harmonic.

Yet another option is an MGU optimized to maximize the brightness at a particular energy, e.g., 8 keV. A device with period length of 17.5 mm and 5 m length, designated MGU17.5, reaches 8 keV with the third harmonic. The shorter period allows more periods in a nominal 5 m length, giving higher brightness. A smaller K may be acceptable, since wide tunability is presumed to not be a requirement.

The reliance on high harmonics (up to the eleventh) puts a premium on magnetic field quality, requiring optical phase error of <2 degrees rms at the fundamental to prevent degradation of brightness of the highest harmonics. We have achieved this level of phase error in the short MGU now installed in the X13 and X29 straights. This level of field quality has also been achieved in longer ID's at other institutions, so it is within the state-of-the-art.

3.4.12.3 Consideration of Radiation Damage in Permanent Magnets

The very low emittance lattices being considered for NSLS-II will have higher beam losses due to lower Touschek lifetimes than the present X-ray ring. The small-gap, in-vacuum MGUs can be expected to intercept a significant fraction of the scattered electrons. Most will be blocked by electron and gamma absorbing apertures placed just upstream of the MGUs. Nevertheless, experience with degradation of permanent magnets reported at APS and ESRF requires that beam loss rates be kept to a minimum, even with the availability of top-off injection.

To deal with permanent magnet degradation, ESRF has abandoned NdFeB in favor of Sm_2Co_{17} for in-vacuum undulators because of its higher radiation resistance. The designers of DIAMOND are following the ESRF lead. Unfortunately, Sm_2Co_{17} has a remanence (B_r) of ~1.05 T, compared to 1.2 to 1.3 T for NdFeB grades currently used in our MGUs and in many out-of-vacuum undulators. Such a low value of B_r would be insufficient to realize the MGUs we are proposing.

Sumitomo Special Metals recently reported their experimental measurement of demagnetization of their type 35EH NdFeB magnets (a high H_{ci} grade used in Spring-8 in-vacuum undulators) when exposed to a 2 GeV electron beam at the Pohang injection linac. After a standard pre-bake at 142^o C for 24 hours, the samples showed a 0.4 % field loss after exposure to 10^{15} electrons. The decrease was linear with exposure. Without pre-bake the losses were even higher. The loss appears to be thermal-like. Experts on permanent magnets in the BNL Materials Science Department confirm that demagnetization by electrons and gammas is probably thermal and, in principle, reversible. (Re-magnetization is, of course, impractical in an assembled undulator, unless one disassembles it and re-magnetizes each magnet individually.)

In another study, Sumitomo found that type 27VH, a super-high H_{ci} grade of NdFeB, degraded about 0.1% at the same exposure, similar to Sm_2Co_{17}. Both 27VH and Sm_2Co_{17} have a remanence of 1.05 Tesla, and similar values of H_{ci}. We can expect that NdFeB with high values of H_{ci} will exhibit equally high radiation resistance as Sm_2Co_{17}.

Fortunately, the mature NdFeB material technology is continuing to improve. Sumitomo Special Metals recently announced the AH series of materials that offer $B_r > 1.3$ T with intrinsic coercivity (H_{ci}) comparable to Sm_2Co_{17}. We therefore expect we can realize the high-performance, radiation resistant, in-vacuum undulators discussed in this proposal.

3.4.12.4 Superconducting Undulators

While the PM based MGUs described in Section 3.4.12.2 meet many of the requirements for NSLS-II, even higher brightness would be possible if the period could be reduced further while still maintaining sufficiently high magnetic field to ensure full tunability. The goal of high brightness and full tunability from the fundamental through the higher harmonics in the 2 to 20 keV spectral range may be achievable with superconducting undulator technology. R&D on superconducting undulators was carried on at the NSLS during the 1990's, in connection with the Superconducting High-Gain Harmonic Generation experiment (collaboration with Grumman Corp) and a Visible Free-Electron Laser project. Superconducting undulator with periods of 26, 18 and even 8.8 mm were built and tested. Figure 3.4.6 shows sections of the 18 mm and 8.8 mm period superconducting undulators.

Recent superconducting undulator designs, derived from this basic concept, have been prototyped at ANKA, LBL and APS. An ANKA innovation is a bifilar helical winding configuration that avoids the multiple 180° bends in the conductor to reverse the winding direction from slot to slot. ACCEL GmbH is now building full-scale superconducting undulators with this design for the Singapore and ANKA light sources

We have used Radia to analyze a magnetic model of a superconducting undulator. The truncated windings are magnetically equivalent in both the parallel and bifilar configurations, as far as field in the gap is concerned. From the model, we find that a period of 14 mm, a gap of 5 mm and an average current density J_c of 1300 A/mm^2 will give 1.6 T peak field, for a K value of 2.28, sufficient for 3:1 tuning range

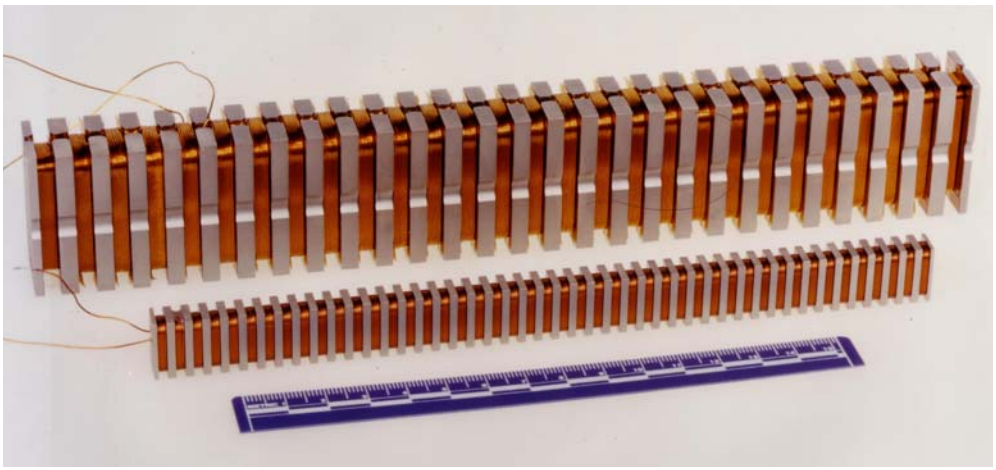

Figure 3.4.6 *Sections of superconducting undulators built at NSLS in the 1990's. The superconductor is wound in machined slots around the iron yokes. The windings are continuous, reversing direction from slot to slot to generate a field of alternating polarity in the iron poles. A pair of such windings facing each other forms an undulator.*

and full spectral coverage. The fundamental energy is 1.58 keV. For coverage of 2 to 20 keV we can utilize the first through the ninth harmonics. The 5 mm gap assumes a thin foil barrier between machine vacuum and insulating vacuum.

An average J_c of 1,300 A/mm^2 is near the limit for conventional NbTi conductors. Higher J_c may be

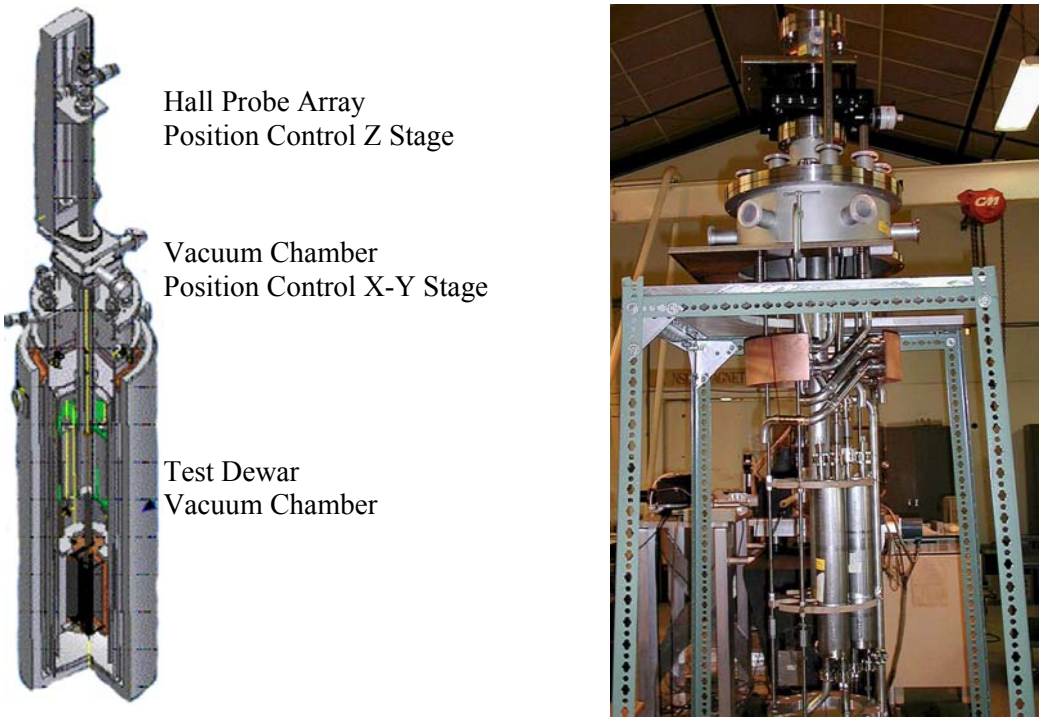

Figure 3.4.7 *(left) Drawing of measurement apparatus for short superconducting undulator models, shown with the Hall probe mapping insert. An interchangable pulsed wire insert is also being designed. Three helium calorimetric circuits are included for detailed heat loss measurements. (right) Photo of measurement apparatus in assembly stand.*

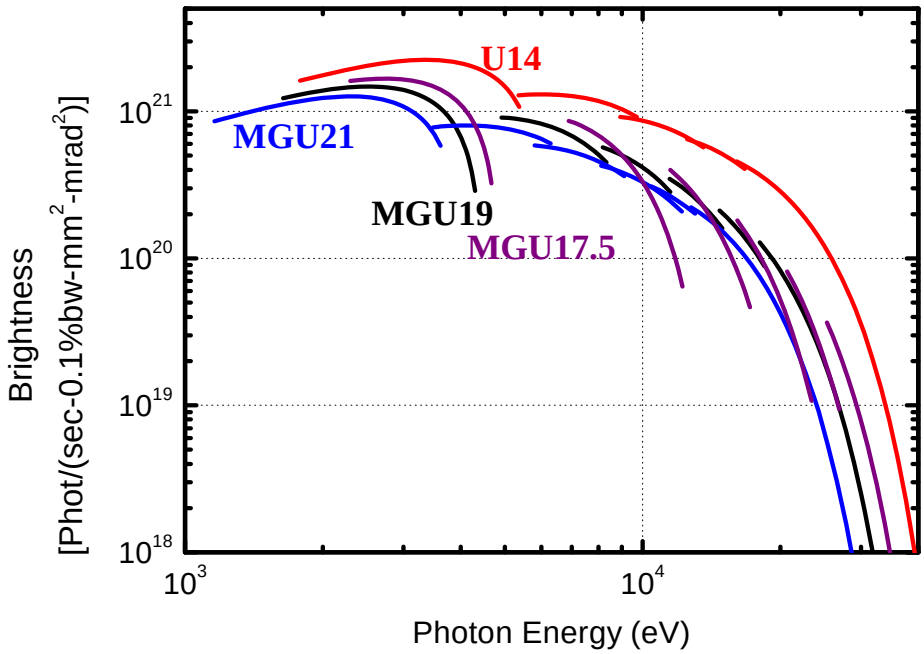

Figure 3.4.8 *Relative performance of the superconducting undulator, U14, compared to that of the permanent magnet undulators MGU17.5, MGU19, MGU21. The superconducting undulator is both brighter and continuously tunable from 2 to more than 20 keV. The first through ninth harmonics are shown for U14 while the first through eleventh harmonics are shown for the MGU devices.*

obtained in NbTi with artificial pinning centers (APC-type), but it is not yet available commercially. $NbSn_3$ is also capable of higher J_c, and practical conductors are becoming available. We will explore conductor options jointly with the BNL Superconducting Magnet Division.

NSLS is continuing its superconducting undulator R&D effort. We are now constructing a magnetic measurement apparatus for magnetic measurement of short superconducting undulator models by both Hall probe and pulse wire techniques. The apparatus will contain calorimetric instrumentation. Both immersion in liquid helium and conduction cooling can be accommodated. It will fit into an existing dewar that we previously used to test our early superconducting undulator models. A schematic drawing and photo of the apparatus is shown in Figure 3.4.7. NSLS is collaborating with BNL's Superconducting Magnet Division, to draw on their expertise and vast experience in superconducting magnet design and construction. Testing and measurement of superconducting undulator models will be performed in the Magnet Division's cryogenic test facilities.

The brightness of a 5 m long superconducting undulator with 14 mm period, designated U14, is compared in Figure 3.4.8 against that of the permanent magnet undulators discussed in Section 3.4.12.2. It is clear that the superconducting undulator is both brighter, by virtue of having shorter periods and hence more periods in a given length, and continuously tunable.

While permanent magnet undulators are today's state of the art, superconducting undulators are tomorrow's state of the art and will be developed as part of the NSLS-II project. The brightness and flux curves for U14 on NSLS-II are shown in Figures 3.3.3 and 3.3.4.

3.4.12.5 Soft X-ray Undulators

Several options are being studied as soft X-ray sources in the 0.2-2 keV range. They include both conventional planar, quasi-periodic and variable polarization undulators. These will be out-of-vacuum

devices. APS-type extruded vacuum chambers may be used, having 5 mm vertical aperture. Allowing for 1 mm chamber walls and 0.5 mm clearance, the minimum magnetic gap for a 6 m long device will be about 8 mm. Extrusions with larger apertures are available for longer ID's.

A conventional planar PM-hybrid undulator with a 40 mm period and 8 mm gap can produce a peak field of 1.27 Tesla for a peak K of 4.7 and fundamental energy of 0.2 keV. A 6 m long device would have 150 full periods. The fundamental, third and fifth harmonics would be used to cover the 0.2-4 keV range. This device is designated U40. Its brightness and flux curves on NSLS-II are shown in Figures 3.3.3 and 3.3.4.

Alternatively, if a somewhat higher energy is range is desired, a similar 6 m long planar PM-hybrid undulator, but with 28 mm period instead of 40 mm period, designated U28, would provide fully tunable high brightness radiation from 0.3 keV to ~ 7 keV from its fundamental, third and fifth harmonics. The brightness and flux of this device on NSLS-II is also shown in Figures 3.3.3 and 3.3.4.

The quasi-periodic undulator (QPU) has the interesting property that higher harmonics are shifted away from integer multiples of the fundamental. This may make it easier to separate higher orders in a monochromator. A pure-PM structure is employed. The quasi-periodicity can be realized in several ways. For example, selected axially polarized magnets may be shorter, or they may be retracted to locally increase the gap.

Variable-polarization undulators come in several varieties. The APPLE-II undulator can provide linear, right- and left circular, as well as any degree of elliptical polarizations. This is accomplished by splitting the conventional pure-PM arrays longitudinally and moving ("phasing") diagonally opposite semi-arrays longitudinally relative to their partners. The lowest energy is reached in the planar, horizontally polarized mode (phase = 0). For other phases that produce elliptical, circular (phase = 90°) and vertical (phase = 180°) polarization modes, the on-axis fields are reduced, so the fundamental resonance occurs at higher energies.

3.4.12.6 Ultraviolet Sources

For vacuum ultraviolet users requiring ten to several hundred eV photons, undulators with very large K values are necessary. The high K also results in very high radiated power in higher harmonics that has to be absorbed by the first optical element in a beamline. The Figure-8 undulator design displaces the radiation of all harmonics above the fundamental off-axis, allowing the possibility of absorbing the unwanted harmonics in a suitable beamstop, while allowing the fundamental to pass through the central aperture. A Figure-8 undulator with 10 cm period can provide photons from 10 to 300 eV in the fundamental. Such a device, 6 m in length and with 10 cm period, is designated U100. Its brightness and flux curves on NSLS-II are shown in Figure 3.3.3 and 3.3.4.

3.4.12.7 Superconducting Wigglers

The highest energy photons (up to 100 keV) are produced by very high field, superconducting wigglers. The radiation is broadband with very high power. Such devices are available commercially with a peak field of up to 5 Tesla. A 1 m long superconducting wiggler with 60 mm period is designated W60. Its brightness and flux curves on NSLS-II are shown in Figures 3.3.3 and 3.3.4.

REFERENCES

[1] Wolski, S. de Santis, Proceedings of EPAC 2002, 524, Paris, France (2002).
[2] P. Elleaume, Nuclear Instruments and Methods, A455, 503-523 (2000).

3.5 Future Upgrade Opportunities

3.5.1 Storage Ring Upgrades

At the present time an electron storage ring is the best steady state source for synchrotron radiation, yielding both high brightness as well as high flux. Most existing storage ring light sources have evolved along several upgrade pathways such as:

- top-off operation
- emittance reduction through the introduction of dispersion into the insertion device straight sections
- richer complement of insertion devices
- higher currents
- longer straight sections

The NSLS-II machine design concept currently incorporates all of these features except the second. Introduction of dispersion in the straight section, which might potentially lower the emittance from 1.5 to ~ 1 nm, will be explored as the lattice design matures. In addition, as discussed in Section 3.4.6, 20 small gap insertion devices are likely to further damp the beam, lowering the emittance. Together, these suggest that it is likely that we will be able to achieve the world's first sub-nm emittance light source.

However, for a major upgrade a new avenue must be pursued. We are exploring the possibility of a converting the storage ring to an energy recovery linac mode of operation in the future as that technology becomes available and mature.

3.5.2 Compatibility with Future Upgrade to Operation as an Energy Recovery Linac

The state of the art NSLS-II is being optimized first and foremost to operate as an ultra high brightness electron storage ring. However, we are exploring the possibilities of upgrading the NSLS-II to an ERL in the future if and when the technology has proven itself and the performance characteristics of the ERL are suitable for our user community.

To function as an ERL, a superconducting linear accelerator would have to be introduced into the NSLS-II complex. Figure 3.5.1 is a schematic illustration of how this might be done in a manner that minimizes the impact on the operation of the NSLS-II storage ring and has the electron beam traversing the linac in the same direction for both acceleration and deceleration as is done in the present generation of ERL prototypes. In addition to the superconducting linac, a recirculating loop consisting of two arcs and transport lines to and from the storage ring would be required, as well as a photoinjector electron source. In this configuration nearly all the beamlines of the NSLS-II could be used "as is" and additional very long insertion devices, able to benefit from the potentially reduced energy spread of an ERL could be added into the recirculating loop.

Some of the technical challenges presented by such an upgrade scheme that will be explored further during the conceptual design phase of the NSLS-II project include:

- the storage ring components (vacuum chamber, IDs, etc) must be capable of accommodating the inherently shorter bunches in an ERL ($\sigma \leq 1$ psec) without damaging the ring or degrading the quality of the electron beam, e.g., heating of small gap IDs in particular superconducting undulators, energy spread increases due to wakefields, coherent synchrotron radiation in the arcs, etc.,

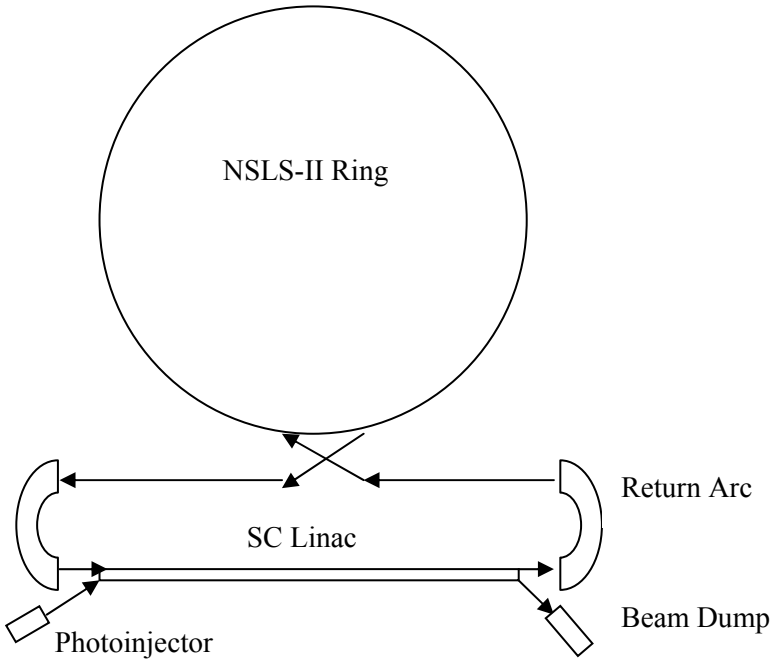

Figure 3.5.1 *Schematic illustration of the general approach which might be used to upgrade the NSLS-II storage ring in the future to operate as an Energy Recovery Linac.*

- the storage ring lattice must have the flexibility to vary the linear and nonlinear momentum compaction in order to control the longitudinal phase space of the ERL beam,
- the shielding and safety systems of the ring must be able to accommodate the "infinite source of charge" characteristic of an ERL,
- the possibility of a "multiturn ERL" in which the beam is kicked into the ring to fill it with charge that is then stored for a fraction of a damping time (a few hundred turns) before being kicked out of the ring and energy recovered; if feasible, this mode of operation can greatly reduce the demand on the photoinjector.

3.6 Facility Siting and Compatibility with BNL's Master Plan

Since NSLS-II is designed to be at the state of the art in terms of photon beam brightness, stability is a significant factor in selecting the site. Because it will be the locus for many lines of cross-disciplinary research at BNL, locating the facility in close proximity to the core research departments is also very valuable. NSLS-II will be a fairly large structure. The preliminary design envisions a building with nearly 350,000 gross square feet (GSF) and a building envelope about 800 feet in outside diameter. Taken together, these factors favor a site just to the southwest of the present NSLS building, as shown in Figure 3.6.1.

The entire area is relatively flat, with less than 20 feet in elevation change from one end to the other. Most of the area is at the same grade within 4 feet of the same elevation, so excavation and filling can be minimized. The soil is undisturbed glacial till, and has few existing utilities running through the area. Locating the building 50 to 100 feet south of Brookhaven Avenue (as shown) is beneficial from the standpoint of minimizing road induced vibration.

The proposed area for NSLS-II is free of any other anticipated program encumbrances. While the 2000 BNL Site Master Plan did not specifically anticipate NSLS-II, it did establish a framework for the development of future scientific buildings, such as the Center for Functional Nanomaterials and NSLS-II, and identified the area shown in Figure 3.6.1 for that development. The BNL Site Master Plan is currently being updated to reflect the intended location of NSLS-II shown in Figure 3.6.1.

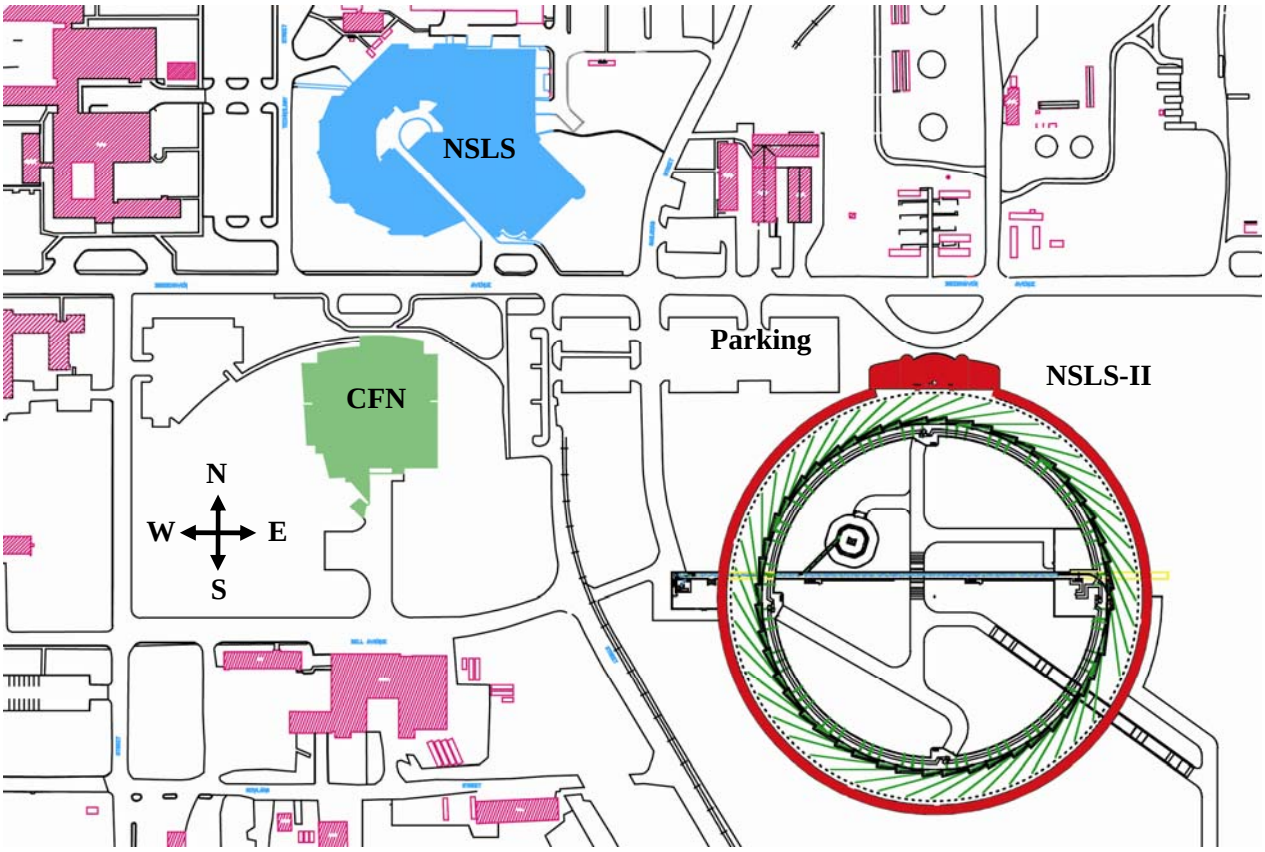

Figure 3.6.1 *Preliminary siting of NSLS-II (outlined in red), located to the southeast of the current NSLS building (in blue) and just east of the BNL Center for Funtional Nanomaterials (CFN) (in green). The area to the south and east of NSLS-II is vacant and available if extra long beamlines extending out from NSLS-II are desired. The Physics, Chemistry, Materials Science, Biology, and Medical Departments and the Instrumentation Division are all nearby.*